Intratumoral heterogeneity and tumor-host crosstalk alter drug sensitivity of clonal subpopulations in a pancreatic cancer model

Eveline E. Vietsch[1]
Sarah Martinez Roth[1]
John K. Simmons[2]
Aamir Javaid[1]
Matthew D. Park[1]
Marianne H.B.C. Stenstra[1]
Justine N. McCutcheon[1]
Eric B. Berens[1]
Ivana Peran[1]
Maha Moussa[1]
Marta Catalfamo[1]
Beverly A. Mock[2]
Giuseppe Giaccone[1]
Marcel O. Schmidt[1]
Anna T. Riegel[1]
Anton Wellstein[1]

[1] *Lombardi Comprehensive Cancer Center, Georgetown University, 3970 Reservoir Road NW, Washington DC 20007, USA*

[2] *Laboratory of Cancer Biology and Genetics, National Cancer Institute, Bethesda, MD 20892, USA*

Submitted

ABSTRACT

Cancers consist of heterogeneous cell subpopulations that survived selection during tumor evolution. Interactions between these subpopulations and the host impact as well as their impact on drug responses are poorly understood. We established a model of tumor heterogeneity using clonal cell lines isolated from a KPC (*Kras*$^{G12D/+}$; *Trp53*$^{R172H/+}$; *P48-Cre*) mouse pancreatic tumor. Deep sequencing of unique mutations characteristic for cancer subpopulations was used to monitor clonal abundance after various anti-cancer therapies in heterogeneous tumors that were reconstituted from cell mixtures. We found that the composition of heterogeneous tumors is affected by the crosstalk amongst the cancer subpopulations and the host environment that includes the immune system as a major player. Some cancer cell subpopulations showed sensitivity to anti-PD-1 immune checkpoint inhibitor treatment in vivo. This sensitivity was mirrored in vitro by the level of activation of T-cells isolated from caecal patches of tumor bearing mice. We provide a platform that comprises the crosstalk between cancer cell subpopulations and the host and reveals the impact on drug efficacy.

INTRODUCTION

Pancreatic ductal adenocarcinoma (PDAC) is a lethal disease for which no curative drug therapy currently exists [1]. The approved drug treatment with the antimetabolite gemcitabine extends disease-free survival after surgery by 6.5 months but does not improve overall survival [2]. Mutant *KRAS*, the major oncogenic driver in PDAC, is present in >90% of tumor specimen [3,4], and acts in part via its downstream effector pathway RAF, MEK and ERK. MEK kinase inhibitors such as trametinib reduce both RAS-dependent MEK and ERK phosphorylation [5]. However, initial studies show that treatment with MEK inhibitors does not provide discernible benefit in patients with PDAC [6], indicating that alternative pathways downstream of KRAS take over during malignant progression [7,8]

DNA sequence and functional analyses revealed that tumors of diverse histological types are composed of clonal cell subpopulations [9-11]. Evolution of these subpopulations is driven by an aggregate of mutations and epigenetic changes as well as selective pressure by the tumor environment [12-17] that is enhanced by the recruitment of cancer-associated stroma and immune cells [18]. Stromal desmoplasia, one of the histologic signatures of PDAC, can inhibit the invasion of cancer cells [19,20] but also plays a role in reducing the efficacy of chemotherapy [21-24] and in suppressing the activity of the immune system [25]. In addition to the stromal / cancer cell interactions, phenotypically different cancer cell populations can influence each other's growth behavior [26-28] as well as treatment responses [29,30].

To establish a model that can track cooperation and competition between cancer subpopulations and the host in response to drug treatment, we generated a series of clonal cancer cell lines from the well-established *LSL-Kras*$^{G12D/+}$; *LSL-Trp53*$^{R172H/+}$; *P48-Cre* driven PDAC model [31]. Genomic analysis revealed that each of the clonal cell lines carries a distinct set of signature mutations. Rather than exogenously tagging cells, we employed these molecular signatures to quantitate the abundance of the clones in reconstituted cell mixtures by deep sequencing of DNA extracted from cells in culture or from allograft tumors in compatible, immune-competent mice. Here we show that growth of subpopulations of cancer cells in heterogeneous mixtures in culture and in tumors and the effects of treatment with an anti-metabolite chemotherapeutic drug (gemcitabine), a MEK kinase inhibitor (trametinib) or an immune checkpoint inhibitor (α-PD-1 antibody) revealed distinct sensitivity of the clonal subpopulations that was affected by intratumoral, stromal and immune cell interactions.

MATERIALS AND METHODS

Mouse experiments

The animal study protocols were approved by the Georgetown University Animal Care and Use Committee. The transgenic KPC mouse model was originally described by Hingorani et al [31]. Mice were aged 3-6 months at time of the experiments and both sexes were used randomly.

KPC derived pancreatic cancer clonal cell line culture

A female KPC mouse 135 days of age was euthanized for tumor harvesting. Fresh mouse pancreatic tumor tissue was minced for 5 minutes and shaken at 150 rpm for 1 hour at 37°C in a Dulbecco's Modified Eagle Medium/Nutrient Mixture F-12 (DMEM/F-12, Gibco Life) with 5% fetal bovine serum (FBS), 2 mg/mL collagenase (Sigma), 4 mg/mL trypsin (Sigma), 50 µg/mL gentamicin (Gibco Life), and 1 IU/mL penicillin/streptomycin (Gibco Life). The cell pellet was washed and centrifuged at 600 g in 4°C in DMEM / F-12, four times. The cell pellet was suspended in primary cell culture media (F-12, 10% FBS, 16 µg/mL insulin (Gibco Life), 10 ng/mL epidermal growth factor, 1 µg/mL hydrocortisone (Sigma), 4 ng/mL cholera toxin (Sigma), 50 µg/mL gentamicin, and 0.5 IU/mL penicillin/streptomycin). The cells were placed in a 37°C, 5% CO_2, humidified incubator on a Collagen-1 coated 10 cm culture dish (Corning BioCoat) in primary cell culture media for 40 minutes to let fibroblasts attach. Subsequently, the unattached cancer cells were transferred to a regular 10 cm dish. Primary cell culture media was changed every 48 hours. Pictures were taken with the Olympus IX71 inverted microscope. After one week, the primary cancer cells were trypsinized, and resuspended in primary cell media in the dilution of a single cell per 200 µL well plated in a 96-well plate. After 3 weeks incubation, eleven wells contained clonal cell populations. The eleven clones were expanded individually to stable clonal cell lines and were grown in DMEM/10% FBS from passage 4 onwards.

3D growth in collagen

One thousand clonal cells were embedded in 40 µL of either neutralized rat tail type-1 collagen (Millipore) / DMEM10% FBS mixture. Cells were left in a 37°C, 5% CO2, humidified incubator for 10 days. Images were taken with using an Olympus IX71 inverted microscope.

Western blot analysis

Protein lysates from cells were obtained using a buffer with 50 mM Tris pH 8.0, 150 mM NaCl, 40 mM β-glycerophoshpate, 0.25% Na-deoxycholate, 1% NP40, 50 mM NaF, 20 mM NaPPi, 1 mM EGTA. Before use of the lysis buffer, 1 mM of Na-orthovanadate and protease inhibitor cocktail (cOmplete, Roche) was added. Protein lysates were prepared for denaturing Bis-Tris gels by adding NuPAGE lithium dodecyl sulfate buffer and Reducing

Agent (Novex, Life), followed by 10 minutes incubation at 70 °C. Proteins were separated in Bis-Tris gels (Novex, Life) by electrophoresis in NuPAGE MOPS SDS Running buffer (Novex, Life). Gels were transferred to polyvinylidene fluoride membranes by the use of the iBlot system (Invitrogen). Membranes were blocked with 5% non-fat dry milk in PBS-T for 1 hour, washed once with PBS-T (0.1% Tween20 in PBS). Primary antibodies (total ERK1/2, Cell Signaling #9102 Rabbit pAb) and phospho T202/Y204 ERK1/2, (Cell Signaling #9101 Rabbit pAb) were diluted to 1:1000 in 5% milk PBS-T. Membranes were incubated at 4 °C overnight. Next, membranes were washed 3 times with PBS-T and incubated with secondary Horseradish peroxidase-linked anti-rabbit antibody (GE Healthcare, NA934V) in 5% milk in PBS-T for 1 hour at room temperature. Membranes were washed 3 times and signals were visualized with Immobilon Western Chemoluminescent HRP Substrate (Millipore) on HyBlot CL autoradiography film (Denville Scientific). Band intensities were estimated using Adobe Photoshop.

RNA sequencing of clonal cell lines

Total RNA was extracted from six clonal cell lines that were grown in DMEM 10% FBS using the RNeasy kit (Qiagen) following the manufacturers' instructions. RNA quality was assessed and all samples had a RNA integrity number (RIN) value higher than 7.0, verified using the 2100 Bioanalyzer (Agilent Technologies). Truseq Stranded RNA libraries were constructed after the depletion of ribosomal RNA using RiboZero. The libraries were then sequenced using the Illumina HiSeq 4000 with paired-end 75 nucleotide reads. Gene expression data in fragments per kilobase of transcript per million reads (FPKM) for every gene in each sample set was analyzed by Gene Set Enrichment Analysis (GSEA), resulting in an enrichment score for each gene when each individual clone was compared to the rest. The scored genes of the experimental data sets were organized into functionality-specific families. The Hallmark family sets represent specific, well-defined biological states or processes based on the Molecular Signatures Database (MSigDB) hallmark gene set collection.

Exome sequencing of clonal cell lines

Genomic DNA from eight samples was analyzed: Six mouse pancreatic cancer clonal cell lines, the corresponding parental KPC mouse tumor tissue and a healthy pancreas from a female p48-Cre littermate mouse. Exome sequencing was performed by Otogenetics (Norcross, GA). In short, mouse exons were captured with an Aligent V4 kit and paired-end 100 nucleotide reads were obtained from the HiSeq2000 (Illumina) with a 30X coverage. Whole exome sequencing data were analyzed was mapped to the MM9 assembly using BWA (v0.7.16a) [32] and the variant calling analysis was performed with HaplotypeCaller as part of the Genome Analysis Toolkit (GATK v3.8-0) [33]. Genetic variants within a given pancreatic cancer clone were then detected by comparison to pancreatic tissue from a the matched, healthy littermate. We focused on non-synonymous mutations only, known

dbSNPs were subtracted. Mutations with less than 5 reads, variant allele frequency less than 0.2, MQ less than 40.00 and genes with more than one mutation were discarded. Unique, clone-specific mutations were validated by Sanger sequencing before using them as clonal signature mutations in later allograft tumor experiments.

Endpoint PCR

DNA from clonal cells and tissue was isolated using the PrepEase Genomic DNA Isolation Kit (Usb), following the manufacturer's protocol. DNA from mouse tissues from different treatment groups was pooled at equimolarity. Per 50 µL of PCR reaction 200 ng of DNA from cells or tissues were used. Endpoint PCR was performed using the Platinum Taq DNA Polymerase Kit (Invitrogen 10966-034), with PCR buffer containing 1.5 mM $MgCl_2$, 0.2 mM dNTP, 0.2 µM primers and 1 U Platinum *Taq* DNA polymerase, using the Epgradient Mastercycler (Eppendorf). The cycling consisted of 2 min at 95 ^{0}C for initial denaturation, 40 cycles of 95 ^{0}C for 30 sec, 61 ^{0}C for 30 sec, and 72 ^{0}C for 40 sec. PCR amplicon products were purified using the QIAquick PCR Purification Kit (Qiagen), removing primers, nucleotides, enzymes, mineral oil, salts, and other impurities from the PCR products. Amplicons were examined by electrophoresis in 2% agarose gel with 1X TAE buffer, and visualized with ethidium bromide and xylene cyanol dye. As a size marker the 1 kb DNA ladder (Invitrogen) was used. The gel was examined under UV light for amplicon bands.

Primers used for PCR amplification of *Kras* and *Trp53* for LoxP genotyping clonal cell lines:

gene	primer	sequence	amplicon size wildtype allele	amplicon size recombined allele
Kras	forward reverse	5'-GGGTAGGTGTTGGGATAGCTG-3' 5'-TCCGAATTCAGTGACTACAGATGTACA-3'	270 bp	304 bp
Trp53	forward reverse	5'- TGACAAGCCTTGCACCTTTCCAAC-3' 5'- CCACAGAGGCTGGATGTGTAA-3'	239 bp	273 bp

Droplet digital PCR for *Kras*^{G12D} allele frequency quantification

DNA from six clonal cell lines was used for PrimePCR ddPCR Mutation Detection (Bio-Rad). Per 20 µL reaction 20 ng DNA were used with ddPCR supermix for probes (no dUTP), 450 nM primers and 250 nM of both *Kras* probes. Probes used for *Kras*^{G12D} allele frequency quantification with ddPCR using genomic DNA from clonal cell lines:

Kras allele	primer	sequence	probe	dye / quencher
wildtype	forward reverse	5'-TATCGTCAAGGCGCTC-3' 5'-GCTGAAAATGACTGAGTATAAA-3'	TGGAGCTGGTGGCG	5'– HEX / 3' – Iowa Black FQ
G12D mutant	forward reverse	5'-TATCGTCAAGGCGCTC-3' 5'-GCTGAAAATGACTGAGTATAAA-3'	TGGAGCTGATGGCGT	5'– 6-FAM / 3' – Iowa Black FQ

The PCR mixture was combined with 40 µL Droplet Generation oil for Probes, and placed in Cartridges in the Droplet Generator (Bio-Rad). Endpoint PCR was performed with the following protocol: Enzyme activation at 95 ^{0}C for 10 minutes, 40 cycles of 94 ^{0}C for 30 seconds, 58 ^{0}C for 1 minute. Enzyme deactivation was achieved at 98 ^{0}C for 10 minutes, hold at 4 ^{0}C. After PCR, the samples were analyzed in the QX200 Droplet Reader to quantify *Kras* allele frequency.

In vitro growth assays

To monitor clonal growth dynamics in vitro, the xCELLigence Real Time Cell Analysis was used as described earlier [34] with 1000 clonal cells/well in DMEM/10% FBS in 16-well E-plates (ACEA Biosciences). All cell lines were measured in quadruplicate wells. For dose response curves the IncuCyte ZOOM system (Essen Bioscience) was used with 250 clonal cells/well plated in 384-well plates in DMEM/10% FBS. After overnight cell attachment, trametinib (Selleckchem) or gemcitabine (LC Laboratories), were added in triplicate wells at different concentrations as indicated in the respective figures. The IncuCyte Zoom system measured Cell Confluence every 12 hours. Growth inhibition was normalized to DMSO control and the respective IC_{50} values were derived by non-linear curve fitting using log [inhibitor] vs. normalized response with variable slope (Prism GraphPad 5.0).

Treatment of pooled mixture of clones in vitro for deep sequencing

Twenty thousand cells per clonal line, to make a mixture of 6 cell lines, were plated in T175 flasks in DMEM10%FBS and allowed to attach for 6 hours. 25 nM of gemcitabine (LC Laboratories) or 100 nM of trametinib (Selleckchem) or DMSO in PBS as a control were added respectively. Cells were allowed to grow to confluency (4 days for the DMSO, 7 days for the trametinib and 11 days for the gemcitabine treated cells). Floating cells were washed away and DNA was isolated from the remaining attached cells after trypsinization.

Growth assay with conditioned media in vitro

Two hundred thousand cells from each of the six clonal cell lines mixed together, or 1.2 million clonal cells alone, were plated in T175 flasks in DMEM10%FBS. After 48 hours, the conditioned media was collected and centrifuged in 0.22 µM membrane vacuum filtration columns (Millipore) to sterilize and remove debris. The conditioned media was stored in 4° Celsius until use. For the growth assay, clonal cell lines G8 and C8 were plated in 16-well xCelligene E-Plates (see above). The cells were plated at a 1:1 ratio of the conditioned media (c.m.) from the clone mix, together with fresh DMEM/10%FBS, or in c.m. from the respective clones (C8 or G8) and fresh DMEM/10%FBS. Different concentrations of trametinib (Selleckchem) or DMSO in PBS as a control were added after cells had attached for 6 hours. The cell index was monitored every 5 hours and dose response curves were generated in Prism Graphpad 5.0.

Allograft tumors

The mouse PDAC cells were tested for mycoplasma contamination and are negative. One million clonal PDAC cells were injected subcutaneously into the flanks of immune competent, compatible wildtype mice (relatives of the KPC mouse). Drug treatments were initiated when tumors had established after ~1 week: 250 µg of rat monoclonal anti-mouse-PD-1 (clone BE0146, BioXCell, New Hampshire, USA) in 50 µL PBS via intraperitoneal injection twice a week, or isotype mAb in PBS as a control; Gemcitabine (LC Laboratories) at 40 mg/kg in sterile water, or water as a control, with 5 doses in week 1 and 2 doses in week 2 by intraperitoneal injections; trametinib (GSK1120212, Selleckchem) by oral gavage at 0.5 mg/kg in 3% DMSO dissolved in 0.5% methylcellulose / 0.2% Tween80 (Sigma) daily for 2 weeks, the carrier mix served as a control.

Histopathology and Immunohistochemistry

Immunohistochemical staining of tumor tissue was performed for α-Smooth Muscle Actin (Rabbit α–SMA monoclonal antibody, Abcam ab124964). Five micron sections from formalin fixed paraffin embedded tissues were de-paraffinized with xylenes and rehydrated through a graded alcohol series. Heat induced epitope retrieval was performed by immersing the tissue sections at 98 °C for 20 minutes in 10 mM citrate buffer (pH 6.0) with 0.05% Tween. Staining was performed using the VectaStain Kit from Vector Labs according to manufacturer's instructions. Briefly, slides were treated with 3% hydrogen peroxide and 10% normal (animal) serum and exposed to 1:1000 Rabbit α–SMA (Abcam ab124964), or α–PD-L1 (Cell Signaling Technology #64988) in Normal antibody diluent (MP Biomedicals) overnight at 4 °C. Slides were exposed to anti-rabbit biotin-conjugated secondary antibody (Vector Labs), Vectastain ABC reagent and DAB chromagen (Dako). Slides were counterstained with Hematoxylin (Fisher, Harris Modified Hematoxylin), dehydrated and mounted with Acrymount. Images were captured using an Olympus IX71 inverted microscope. Histopathological evaluations were done with advice from pathologist Dr. Bhaskar Kallakury.

Amplicon deep sequencing

The six genes with clonal signature mutations were PCR amplified and validated by Sanger sequencing (MCLab). Purified PCR amplicons of these clonal signature genes plus mutant *Kras* and mutant *Trp53* for all cancer cells were from DNA from allograft tumors that were pooled in equimolarity. PCR amplicons were quantified using the Quantifluor ONE dsDNA kit on the GloMax-Multi-Plus Microplate Reader (Promega) by following the manufacturer's protocol. Amplicons were used for MiSeq deep sequencing. Primers used for PCR amplification of the eight genes containing clonal and ubiquitous cancer cell signature mutations:

gene	primer	sequence	variant [mm9 position]	amplicon size
Trp53 (ubiquitous)	forward reverse	5'- GAAAGGGAGGAAGAAGGAAAG-3' 5'- CTTCCAGATACTCGGGATACA-3'	chr11:69402014 G>A	492 bp
Kras (ubiquitous)	forward reverse	5'-TGGACTTTCTTGCACCTATGG-3' 5'-AGTGTTGATGAGAAAGTTGTAAGTG-3'	chr6:145195291 C>T	481 bp
Olfr1157 (C8)	forward reverse	5'- TCTTAGATTTGGGAAGACCTTACA-3' 5'- CCCACCTCACAGTCATCATT-3'	chr2:87802181 G>C	494 bp
Nox4 (D10)	forward reverse	5'- GAGCACTTGGCAATGTAAGAATAG-3' 5'- CCCAGAATAACCCACTCACTAAA-3'	chr7:94462586 C>T	493 bp
Matn4 (F2)	forward reverse	5'- GCACATACACACCACCATCT-3' 5'- GCTACACTCAGAAGTGACATCC-3'	chr2:164222680 C>T	481 bp
Baiap3 (C5)	forward reverse	5'- GTAGGAGCCTTACAACAGGAAG-3' 5'- GCTAGTTGACTGGCAACAGTA-3'	chr17:25387359 G>T	500 bp
Arhgap25 (G8)	forward reverse	5'- GCTCCTTGTTCTCCTGAATCC-3' 5'- CATACACGTGATACCCAGACATAC-3'	chr6:87426299 T>C	497 bp
Pla2g4d (G9)	forward reverse	5'- AAGTTCCAGGATAGCGACAAG-3' 5'- GATCCTTGGATTCCCTTGGAG-3'	chr2:120094626 G>T	502 bp

Amplicons were pooled according to their sample type after quantitation as above. Pooled amplicons were normalized to a concentration of 10 ng/μL, and then diluted further to 0.2 ng/μL in nuclease free water. Library construction: Each amplicon pool was constructed into a library using the Nextera XT DNA library preparation kit (Illumina). Briefly, 1 ng of each amplicon pool was enzymatically sheared and simultaneously tagged with an adapter. A unique index sequence was added to each library sample through a 12-cycle PCR amplification. Each sample was purified and size selected to capture greater than 500 bp amplicons using AMPure XP beads. Quality of the indexed libraries was assessed using the High Sensitivity DNA kit on the 2100 Bioanalyzer system (Agilent Technologies). The libraries were normalized and pooled together by following the Nextera XT DNA user guide (Illumina).

MiSeq sequencing and data analysis

Before sequencing, an aliquot of the library pool was denatured at 96°C for 2 minutes and then kept on ice. One percent of 12.5 pM PhiX Control V3 (Illumina) was spiked into the denatured library pool. Paired end 2x150 bp sequencing was performed on the MiSeq using the MiSeq Reagent Nano kit v2 (300 cycles) according to the manufacturer's protocol (Illumina). All primary- and run-quality analyses were performed automatically on the MiSeq. Alignment to the mus musculus genome 9, NCBI 37 assembly (mm9) and quality trimming were executed by the Burrows-Wheeler Aligner tool on the MiSeq. All point mutations specific to each sample were reviewed by manual visualization of the reads in the Integrated Genomics Viewer (Broad Institute) and variant allele frequencies (VAF) were quantified. Clonal abundance in the tumors was normalized to the VAF of $Trp53^{R172H}$, to account for

wildtype stroma in the tumors. The minimum VAF for clone specific genes was set to 0.01%, in case the clonal mutations were below detection.

qRT-PCR analysis

RNA from allograft tumors was isolated using the RNeasy Mini Kit (Qiagen) following the manufacturer's protocol. 500 ng of RNA was used for complementary DNA synthesis with the iScript cDNA synthesis Kit (BioRad), with 4 µL reaction mix, 1 µL reverse transcriptase in a 20 µL reaction. The Epgradient Mastercycler (Eppendorf) cycling consisted of 5 min at 25 °C, 30 min at 42 °C, 5 min at 85 °C, hold at 4 °C. Next we performed qRT-PCR in a 20 µL reaction using the iQ SYBR Green Supermix (BioRad), containing 10 µL of SYBR Green mix, 1 µL of cDNA and 200 nM primers for the following mouse genes: (β-Actin forward primer GGCGCTTTTGACTCAGGATTTAA, β-Actin reverse primer CCTCAGC-CACATTTGTAGAACTTT; *α-SMA* forward primer GTCCCAGACATCAGGGAGTAA; α-SMA reverse primer TCGGATACTTCAGCGTCAGGA. The Realplex2 Mastercycler Epgradient S (Eppendorf) cycling consisted of 3 min at 95 °C, and 40 repeats of 15 sec at 95 °C, 30 sec at 60 °C, 20 sec at 68 °C. Data analysis was performed with Prism 5.01.

Flow Cytometry analysis of leukocytes in allograft tumors

The mixture of 6 clonal PDAC cell lines (1 million total) or individual clonal cell lines were injected subcutaneously into immune competent wildtype mice, and allograft tumors were allowed to grow for 10 days before tumor tissue collection. Single cell suspensions were generated by mechanic and enzymatic digestion of tumor tissues. Cell suspensions were washed and 1-2 million cells were stained as follows. Cells were labeled for Live/Dead (Invitrogen, Thermofisher, Ref: l-23105) followed by blockade of Fc receptors with CD16/CD32 (clone 2.4G2; BD Biosciences, 553141). After 10 minutes incubation, cells were stained with a cocktail of mAbs: anti-mouse-CD45 (clone 30-F11; 564590), NK-1.1 (clone PK136; 562864), B220 (clone RA3-6B2; 563103), CD3e (clone 145-2C11; 564661), CD4 (clone RM4-5, 563151), CD8a (clone 53-6.7, 564920), PD-1 (clone J43; 744549), CD25 (clone PC61; 565134), all from BD Biosciences. Cells were acquired with FACS Symphony, BD Biosciences and analyzed with FlowJo and Prism Graphpad 5.01.

Mouse caecal patch T-lymphocyte isolation

The mixture of 6 clonal PDAC cell lines (1 million total) was injected into the peritoneal cavities and subcutis of immune competent wildtype mice, and pancreatic tumors were allowed to grow for 2 weeks. After euthanasia, ceacal lymphoid patches were harvested resected in a sterile hood, then cut and shredded in 4 mL of sterile PBS containing 2% FBS and 1 mM EDTA. The cell suspensions were collected in gentle Macs C tube (cat. # 130-093-237) and further dissociated with the gentleMACS (Miltenyi Biotec) for 15 minutes as following: Loop, Spin 150 rpm 2 min, Ramp 400 rpm 30 sec, End loop. In a sterile hood,

remaining aggregates were removed by passing cell suspension through a 70 µm mesh nylon cell strainer cap (BD Falcon) into a 5 mL Polystyrene round bottom tube. The cells were centrifuged for 5 min at 200 x g, supernatant was aspirated and cells resuspended in 1.5 mL fresh PBS containing 2% FBS and 1 mM EDTA. T-lymphocytes were isolated using the EasySep Mouse T Cell Isolation Kit (Stemcell Technologies), according to the manufacturer's protocol. In brief, per 1.5 mL sample, 75 µL Rat Serum was added, in addition to 75 µL Isolation Cocktail. The samples were inverted 15 times and left at room temperature for 10 minutes. RapidSpheres were vortexed and 112 µL was added per sample. The samples were inverted 15 times and left at room temperature for 2.5 minutes. The samples were gently mixed by pipetting and placed inside the EasySep Violet Magnet (StemCell Technologies) for 2.5 minutes at room temperature. The T-lymphocyte suspensions were poured into sterile 15 mL Falcon tubes. Live T-lymphocytes were quantitated using Countess cell counting chamber slides (Invitrogen), and Trypan Blue stain (Invitrogen) with the Countess.

T-lymphocyte culture in vitro

The T-lymphocytes were centrifuged at 100 x g for 5 minutes, and after aspiration of the supernatant, the T-cells were suspended in RPMI (Gibco Life) with 10% fetal bovine serum, 100 units/mL penicillin and 100 µg/mL streptomycin, and 30 units/mL mouse recombinant Interleukin-2 (StemCell Technologies). The cells were plated in 96-well plates (~20,000 live T-cells per well) and placed in a humidified 37°C, 5% CO_2 incubator. As pilot experiment, 100 cancer cells of the equal mixture of the 6 PDAC clonal cell lines were added and incubated for 72 hours. In the following experiment, 1500 clonal cancer cells per well were added to the T-cells, together with 20 µg/mL rat monoclonal anti-mouse-PD-1 (clone BE0146, BioXCell) or 20 µg/mL isotype igG2a (BioXCell).

As the control condition of activated T-lymphocytes, the wells were incubated with 5 µg/mL hamster anti-mouse-CD3e (eBioscience) in sterile PBS overnight before T-cell isolation, whereafter T-lymphocytes were incubated with 30 units/mL mouse recombinant Interleukin-2 and 2 µg/mL hamster anti-mouse-CD28 (eBioscience). After 72 or 48 hours of T-cell incubation in vitro, images were taken with using an Olympus IX71 inverted microscope. The conditioned media was collected in 1.5 mL microcentrifuge tubes and spun down for 5 min at 300 x g. The supernatant was stored at -80 ° Celsius in 100 µL aliquots until further analysis.

ELISA for mouse IFN-γ in the supernatant of T-lymphocytes

Supernatant from the T-cells was thawed on ice. IFN-γ was measured in 100 µL supernatant per condition using the Mouse IFN-γ ELISA Ready-SET-Go! Kit (Invitrogen), following the manufacturers' protocol. In brief, a Corning Costar 9018 ELISA 96-well plate was coated with 100 µL/well of capture antibody in 1X Coating Buffer. The plate was sealed and incu-

bated overnight at 4° Celsius. Wells were washed with 250 µL 0.05% PBS-T (wash buffer) 3 times. Wells were blocked with 200 µL 1X ELISA Diluent for 1 hour at room temperature. After washing once with wash buffer, 100 µL of the T-cell supernatant was added to the wells, or RPMI-10% or 1X Diluent as controls. The mouse IFN-γ standard was serial diluted in 1X Diluent from 4,000 to 4 pg/µL. After 2 hours incubation at room temperature, the wells were washed with wash buffer 5 times. Detection antibody in 1X Diluent was added to the wells in 100 µL incubated at room temperature for 1 hour. After 4 washes, 100 µL/well of Avidin-HRP* diluted in 1X ELISA/ELISPOT was added to the wells and incubated at room temperature for 30 minutes. Wells were washed 7 times before adding 100 µL/well of 1X TMB Solution. The plate was incubated at room temperature protected from light for 15 minutes. The reaction was stopped with 50 µL 1 M H_2SO_4 per well. Luminescence was measured at 450 nm using the Victor2 Wallac reader (Perkin Elmer).

RESULTS

Isolation of clonal cell lines from a mouse PDAC model

Genetically engineered mouse models (GEMM) can recapitulate human pancreatic ductal adenocarcinoma (PDAC) pathology. In particular, the LSL-*Kras*$^{G12D/+}$; LSL-*Trp53*$^{R172H/+}$; *P48-Cre*, (KPC) model [31], mimics the genomic instability and disease progression, including metastases, of human PDAC. In addition to the heterogeneity of primary pancreatic tumors in the KPC model, diaphragmatic and peritoneal metastases are polyclonal [35]. However, clonal variants within a single pancreatic tumor derived from this model have not been characterized in depth.

To model intratumoral clonal heterogeneity, we established clonal cell lines from a primary PDAC lesion of a KPC mouse (Fig. 1a). The primary tumor showed the characteristic ductal adenocarcinoma and desmoplastic histopathology (Fig. S1a), and the liver and lungs of the KPC mouse contained metastatic lesions (Fig. S1b). After a brief expansion of the primary PDAC cells from multiple tumor regions in 2D cell culture, we generated eleven clonal cell lines by single cell cloning (Fig. 1a). Genotyping of the clonal PDAC cell lines confirmed heterozygosity for the *Kras* locus (wildtype and recombined *Kras*) and a loss of the wildtype *Trp53* allele (Fig. S1c), similar to previous assessments of PDAC cells from KPC mice [31].

The clonal PDAC cell lines are polymorphic and genetically heterogeneous

From the initial cell line panel we selected six cell lines with distinct cell morphology and 3D growth phenotypes: The clones D10 and F2 are spindle-shaped, whereas C5, G8 and G9 display cuboidal morphology (Fig. S1d).

To evaluate signal transduction downstream of mutated KRAS, we assessed ERK1/2 phosphorylation in the individual clones by Western Blot analysis. Different levels of phospho ERK1/2 in the clonal cell lines grown in vitro (Fig. 1b) indicate distinct stimuli in addition to the presence of the *Kras*^{G12D} oncogenic driver mutation. Differences in the *Kras*^{G12D} variant allele frequency (VAF) of 1:1 to 4:1 (Fig. S1e) did not match with the different levels of ERK phosphorylation. This corroborates previous studies showing that *KRAS* mutation status is only poorly related to ERK activation [36-38], and suggests additional, distinct regulators of ERK1/2 activity amongst the clones derived from the same *Kras*^{G12D} driven tumor.

Collagen can reveal invasive behavior of pancreatic epithelial cells [39-41] and we assessed whether the clonal PDAC cell lines show different formation of ductal structures during 3D growth in type 1 collagen. The ability to develop ducts was poor for clones G8 and G9, whereas clone C5 formed wide ducts with blunt terminal buds, and C8 and F2 generated meshes of thin tubules (Fig. 1c).

Distinct gene expression patterns were found for the clonal cell lines grown in vitro by RNA sequencing. When comparing the clonal gene expression values to the average expression of all six clones, we found that clone G9 had the highest number of differentially expressed genes with 90 genes being upregulated more than 2-fold and 179 genes being down regulated. The lists of genes can be found in Data file S1. Gene set enrichment analysis was performed and the Hallmark Pathway families that were distinct for the clonal cell lines are shown in Figure 1d.

Next we assessed the genomic heterogeneity using whole exome sequencing of DNA from the parental tumor tissue and from the six individual clonal cell lines. To avoid contamination by circulating or metastatic cancer cells, genomic DNA from a tumor-free pancreas of a healthy female littermate mouse was used as a control. In the parental tumor tissue 174 non-synonymous that lead to amino acid substitutions were detected. The lists of mutations in the clonal cell lines and the tumor are shown in Data file S2. The clonal cell lines contained 146-247 mutations (Fig. 1e). Based on the multicellular oncogenic activation, the KPC model gives rise to multifocal cancer [35]. We found 64 ubiquitous mutations that are shared among all clonal cells and the parental tumor (Table S1), supporting the notion that the clonal cells were derived from a common ancestor that was selected for at an earlier stage of tumor progression. Approximately half (45% to 67%) of the mutations found in the clonal cell lines were detectable in the tumor tissue at the sequencing depth applied to the genomic DNA. The different abundance of the clonal subpopulation in the tumor tissue as well as the dilution of the tissue DNA by stromal cell DNA explains that not all of the mutations found in the cell lines were also detectable in the original tumor tissue. The number of unique mutations range from 18 in C5 and G8 to 89 in clone C8 (Fig. 1f). The list

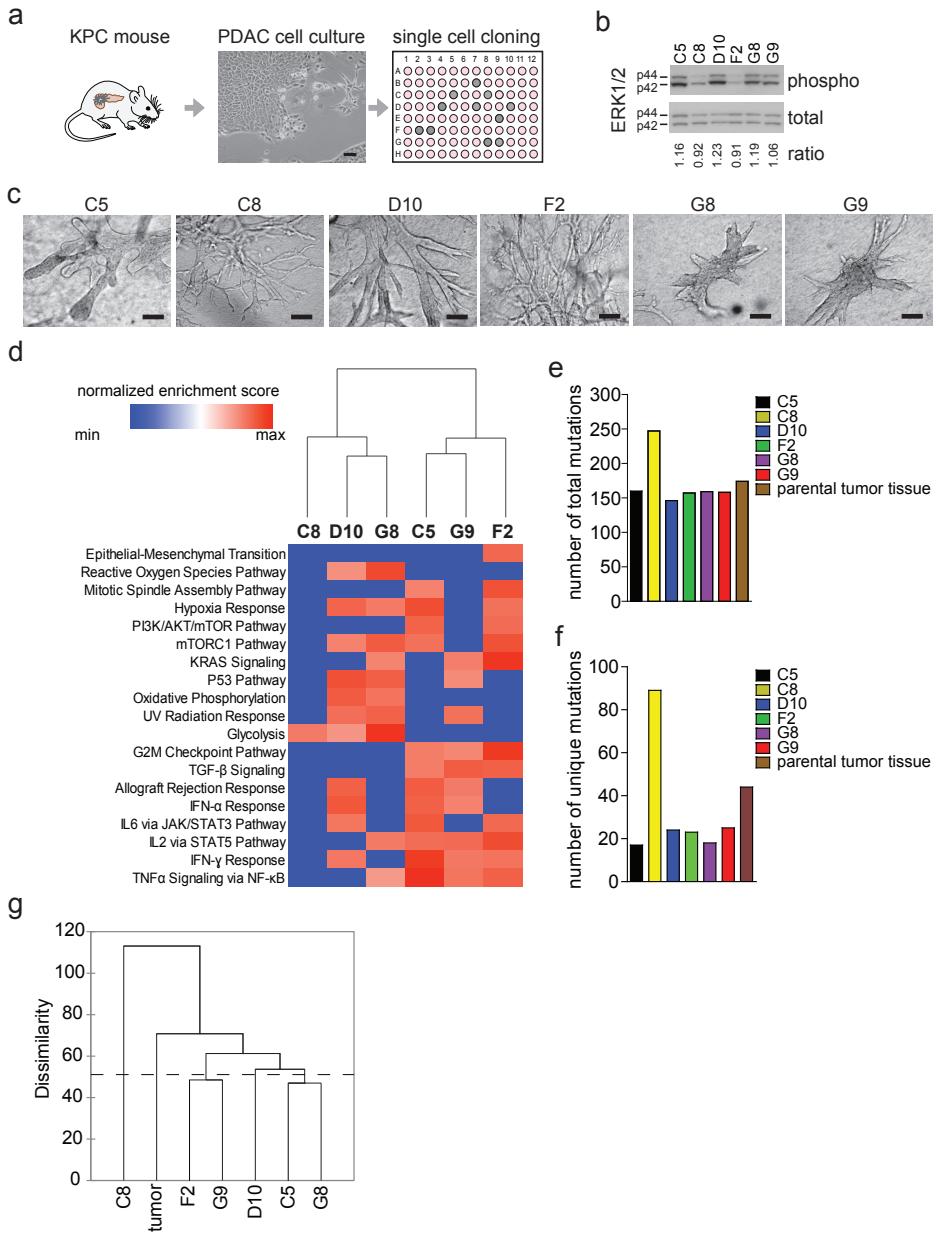

Figure 1. Characterization of clonal cell lines from a KPC mouse pancreatic tumor.

a. Workflow for the generation of clonal cell lines. A pancreatic tumor from an LSL-*Kras*$^{G12D/+}$; LSL-*Trp53*$^{R172H/+}$; P48Cre/- (KPC) mouse was harvested and cultured for one week. An image of the primary cancer cell growth is shown (scale bar = 100 µm). When the culture reached confluence, cells were transferred to a 96-well culture plate for single cell cloning. After 3 weeks of incubation eleven wells contained clonal cell lines (grey circles).

b. Western blot for phospho ERK1/2 (Thr202/Tyr204) and total ERK1/2 protein in clonal cell lines.

c. 3D tubular structures of clonal cell lines grown in collagen-1 for 10 days. Scale bar = 100 µm. Equal numbers of the clonal cells were grown as 2D monolayers in DMEM 10%FBS for 3 days.
d. Heatmap of the Hallmark Pathway Families of the clonal cell lines in vitro, based on Gene Set Enrichment Analysis (GSEA) of RNA-sequencing gene expression data.
e. Number of non-synonymous single nucleotide variations in the clonal cell lines and the parental tumor tissue detected by exome sequencing.
f. Number of unique signature mutations in the clonal cells and the parental tumor tissue.
g. Cluster analysis of the gene mutations in the clonal cells and the parental tumor tissue. The dashed line indicates significant differences (Euclidian distance).

of unique signature mutations is shown in Table S2. Cluster analysis of the mutations show the relationship between the tumor tissue and the clonal cells and Indicates that clone C8 is most distinct (Fig. 1g).

In summary, we found that the KPC tumor harbors genetically distinct cancer subpopulations, that matches with previous studies in both murine and human PDAC [11,35,42,43]. In the experiments described below we took advantage of the unique mutations in individual clones, to track and quantitate their abundance in clonal mixtures in cell culture as well as tumor growth in vivo.

In vitro drug responses of the clonal PDAC cell lines are distinct

To uncover potential differences in growth pathway activity of the clonal cell lines we evaluated their sensitivity to different drugs. Monolayer growth of the clonal cell lines shows some differences in the growth rates as well as at the maximum level of confluence, as indicated by the impedance measurement (Fig. 2a). Clone G8 has the highest growth rate compared to the other clones (Fig. 2b). We next assessed the sensitivity of the clonal cell lines to gemcitabine that is the approved for the treatment of PDAC, and evaluated the response of the clonal cell lines to a series of pathway-targeted drugs. Initially, 196 kinase inhibitors that target >34 kinases were tested for their growth inhibitory effect at a fixed concentration of 500 nM (data not shown). From this screen, we found that drugs targeting MEK, a RAS-effector known to be activated in human *KRAS* mutant PDAC [44] distinguished best between the clones. We also included the anti-metabolite gemcitabine in the analysis since it is approved for the treatment of PDAC. Dose response curves of treatment with gemcitabine and the clinically used MEK inhibitor trametinib (Fig. S2a) showed IC50 values ranging from 15 to 205 nM between the clonal cell lines in vitro (Fig. 2c). Gemcitabine was not as selective, with IC50 values ranging from 5 to 19 nM (Fig. 2c). These distinct sensitivities to anti-cancer drugs with different mechanisms of action amongst cell subpopulations from the same tumor indicate the functional heterogeneity of growth pathway activity in the clonal cell lines. There was no correlation between gemcitabine or trametinib sensitivity and the proliferation rates or the levels of ERK1/2 phosphorylation of the individual clones.

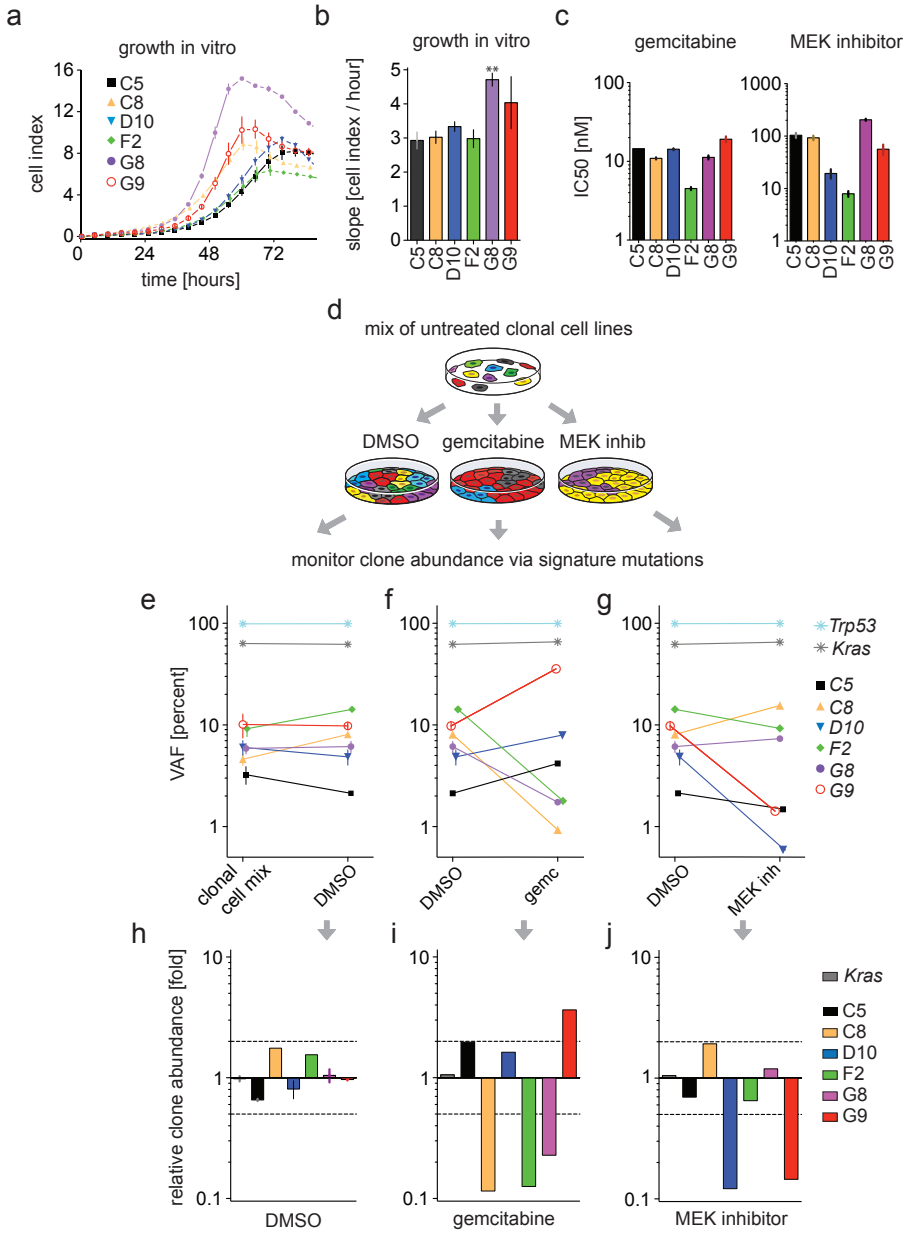

Figure 2. Clonal drug sensitivity in the context of the mixed population in vitro.

a. Cell growth of the individual clonal cell lines in vitro. Error bars are SEM of 4 replicate wells.

b. Growth rates of individual clonal cell lines in vitro. Slopes of growth curves were calculated from the data in Fig. 2a, with error bars representing the SEM of 4 replicate wells. ** P =0.0024 by t-test relative to other clonal cell lines.

c. IC_{50} values of individual clonal cell lines after a 72 hour treatment in vitro with gemcitabine or trametinib, calculated from the dose response curves shown in Suppl.Fig 2b. Error bars represent SEM of drug treated cell growth in triplicate wells. Note: log scale of the Y-axis

d. Schematic depiction of the growth assay of the clonal cell mixture in vitro in the presence of DMSO, 25 nM gemcitabine or 100 nM trametinib. When cells reached 90% confluency, genomic DNA was extracted to measure clone abundance by deep sequencing.
e - g. Variant allele frequencies (VAF) of *Kras*, *Trp53* and 6 genes containing clone-specific signature mutations, measured by amplicon deep-sequencing. DNA from the untreated cell mix and the clone mixture grown in presence of DMSO (e), the clone mixture grown in presence of DMSO or gemcitabine (f) or trametinib (g) until confluent. Note the log scale of the Y-axis. Three and two sequencing runs were carried out for the starting clone mixture and DMSO treated cells respectively.
h - j. Change in clone abundance after treatment with DMSO (h), gemcitabine (i) or trametinib (j) based on the VAFs of the clonal signature mutations, compared to those in the starting clone mix. Note the log scale of the Y-axis. The dashed lines indicate 2-fold increase or decrease in clone abundance.

In vitro drug responses of clonal cells are altered when growing in the heterogeneous cell mixture

As a step towards the analysis of a heterogeneous cancer cell population, we next assessed the drug sensitivity of individual clones in the mixed population (Fig. 2d). We hypothesized that resistant clones in the population would have a selective advantage though the crosstalk between different clones via secreted factors or cell-cell contact might impact the sensitivity to pathway inhibitors. Deep sequencing for the signature mutation of each clone (Table 1) was employed to identify and quantitate the abundance of clones in the mixture. The number of reads of mutant and wildtype DNA are shown in Table S3. Variant allele frequencies (VAF) measured in the starting mixture of the clones were compared to those in the clone mixture that had grown under control conditions (DMSO) or gemcitabine (25 nM) or trametinib (100 nM) until reaching confluence (Fig. 2d). The VAFs under control and drug treatment are shown in Fig. 2e-g and the impact of drug treatment on the clonal contribution to the cell population in Fig. 2h-j. It should be noted that each cell line retains only one copy of the *Trp53* allele, with the R172H mutant, that is reflected in the ~100% read of the VAF for *Trp53*, irrespective of the treatment.

Table 1. Genes with signature mutations used to identify clones by deep sequencing.

clone	gene	chrom	position (mm9)	heterozygous variant	AAS	transcript
C5	*Baiap3*	chr17	25387359	G>T	L170I	NM_001163270
C8	*Olfr1157*	chr2	87802181	G>C	I289M	NM_146849
D10	*Nox4*	chr7	94462586	C>T	T89M	NM_015760
F2	*Matn4*	chr2	164222680	C>T	R339Q	NM_013592
G8	*Arhgap25*	chr6	87426299	T>C	K171R	NM_001037727
G9	*Pla2g4d*	chr2	120094626	G>T	S710R *	NM_001024137
Each clone	*Trp53*	chr11	69402014	G>A	R172H ^	NM_001127233
Each clone	*Kras*	chr6	145195291	C>T	G12D	NM_021284

chr = chromosome; mm9 = mus musculus reference genome 9; AAS = amino acid substitution;
* = mutation also present in the parental tumor tissue; ^ = loss of wildtype allele

When the mixed cancer cell population was grown under control conditions, no significant enrichment of clones was found (Fig. 2h). This was surprising since clone G8 grows significantly faster than the others when grown individually. Paracrine signaling may harmonize the growth rate of clones in the mixture. Gemcitabine treatment, selected for clone G9 by ~4-fold and led to a ~5-10-fold decreased abundance of clones C8, F2 and G8 (Fig. 2i). The latter 3 clones were the most sensitive to gemcitabine (Fig. 2c) and their reduced abundance matches with their relative sensitivity to the drug. This indicates that cancer cell crosstalk had no major impact on the effect of gemcitabine, in line with the cell-autonomous mechanism of action of this anti-metabolite.

In contrast to gemcitabine, treatment with trametinib led to a ~10-fold reduction of clones D10 and G9 in the mixed population (Fig. 2j). Clone C8 made up the largest portion of the population (Fig. 2f) and therefore seems unresponsive to trametinib when grown in the presence of the other clones. To our surprise, the most MEK inhibitor-resistant clone G8 (Fig. 2c) did not dominate when growing in the presence of the other cell lines and trametinib (Fig. 2j). To assess whether secreted factors from the other clones played a role in sensitizing clone G8 to trametinib, we conducted an experiment with conditioned media. As a comparison we used clone C8, which appeared favored by 2-fold when the mixture was treated with trametinib. Clonal cell lines G8 and C8 were grown individually and treated with different concentrations of trametinib in the presence of conditioned media from the matching cell line, or with the conditioned media from the mixed population. We found that clone G8 is sensitized to trametinib when conditioned media from the mixed population was added (Fig. S2b) but did not observe this effect for clone C8 (Fig. S2c). We conclude from this that growth behavior and drug sensitivity of cancer cell subpopulations can be altered by the composition of the population due to paracrine crosstalk.

Tumorigenesis of clonal cell lines in immune competent mice

When placed in the intraperitoneal cavity of immune-competent compatible mice, each clonal cell line homes to the pancreas, invading and destroying the tissue architecture (Fig. S3a). To easily monitor the tumor growth rate, the individual clonal cell lines were also injected subcutaneously into the flanks of compatible mice. It is noteworthy that the histopathological features of the subcutaneous tumors were indistinguishable from those of orthotopic allograft tumors in the pancreas (Fig. S3b vs S3a). In vivo, clone D10 the most fibroblast-like clone (Fig. S1d), generates poorly differentiated tumors, whereas the other clones developed differentiated adenocarcinomas with glandular structures, either orthotopically or subcutaneously. Differentiation of the tumors was not predictable from the 3D growth phenotype of the clonal cell lines in collagen type 1, in which D10 forms tube-like structures, whereas G9 and G8 do not (see Fig. 1c). Growth rates of the subcutaneous clonal tumors from C5 and D10 were relatively low, whereas clone G8 grew at a significantly

higher rate than the other clones (Figs. 3a, S3c). Interestingly, gene analysis indicated an upregulation of the allograft rejection response pathway for clones C5 and D10 (Fig. 1d) and corroborates the tumor growth phenotype. All clones recruited cancer-associated fibroblasts and induced desmoplasia that is pathognomonic for PDAC. Staining of the tumors for α-smooth muscle actin (α-SMA) revealed equal proportions of myofibroblasts across the subcutaneous allograft tumors from the clonal cell lines (Fig. S3d). The homogeneous recruitment of myofibroblasts was confirmed by qRT-PCR analysis of the gene expression levels of α-SMA in the clonal allograft tumors (Fig. S3e).

Response of heterogeneous tumors to different types of drug therapy

Tumor tissue architecture has profound effects on malignant progression and resistance to drug therapy and is controlled by cell-cell and extracellular matrix interactions [19,20,43]. In addition, cytotoxic drugs and pathway inhibitors can stimulate or inhibit stromal cells that participate in the immune response to a malignant lesion [45-47]. To assess treatment responses of PDAC subpopulations in the context of tumor stroma and an intact immune system, we inoculated compatible, immune-competent syngeneic mice with an equal mixture of the above described six clonal cell lines and treated them with prototypic drugs that target different hallmarks of malignancy. We hypothesized that the relative drug sensitivity of clonal subpopulations would be distinct for drugs that act via different mechanisms. Also, we surmised that clonal responses in vitro might differ from the in vivo sensitivity due to host-tumor interactions. The heterogeneous subcutaneous tumors were allowed to establish for one week and mice were then treated for two weeks with intraperitoneal injections of the control (PBS containing DMSO or control IgG), gemcitabine, an anti-programmed death-1 (PD-1) antibody, or oral gavage with trametinib (Fig. 3b). The maximal inhibitory effect on tumor sizes after gemcitabine and trametinib was reached after 5 days of treatment, whereas the α-PD-1 was most effective in reducing tumor size after 10 days of treatment (Fig. S4a). At the end of the two-week treatment period tumors were harvested for evaluation.

Distinct impact of different drugs on the allograft tumor stroma

The impact of stroma is crucial in cancer growth and known to modulate drug responses. Thus we initially evaluated the impact of drug treatment on the tumor cell/host stroma ratio. For this, we took advantage of the fact that the wildtype *Trp53* allele is lost from the cancer cell lines and used the *Trp53*^{R172H} variant allele frequency (VAF) as the readout of cancer cell abundance in the tumor tissues (Fig. 3c). Given that stromal cells from the host carry two copies of the wildtype *Trp53* allele and the cancer cells only one copy of mutant *Trp53*^{R172H}, an equal contribution of stromal and cancer cells to the tumor would result in a *Trp53*^{R172H} VAF of 33.3%. We observed a ~50% VAF indicating that 2/3 of the tumor mass is contributed by cancer cells. Although histologically the stroma appears dominant, this is mostly due to desmoplasia and not the abundant presence of stromal cells. After gemcitabine

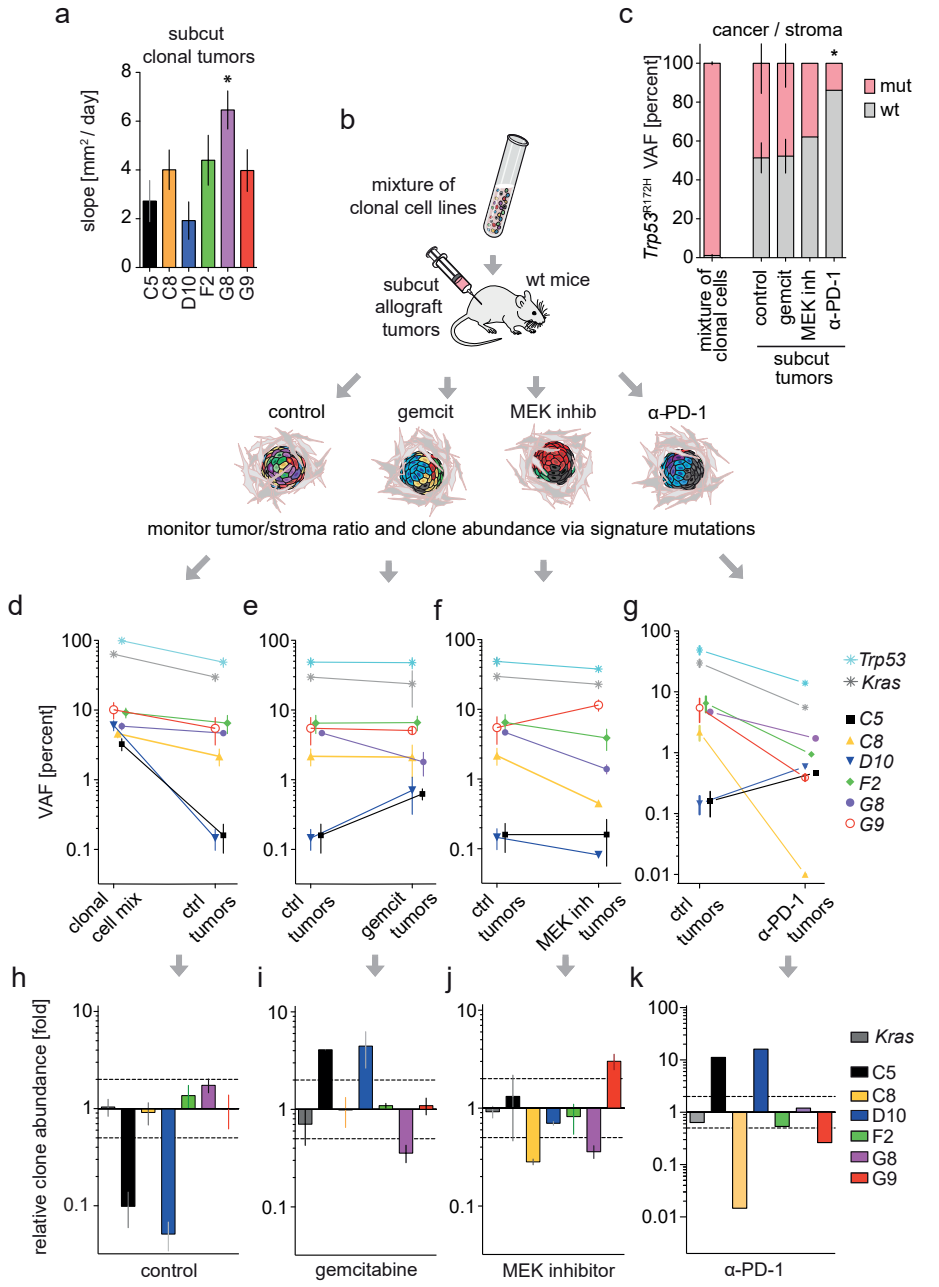

Figure 3. Clonal drug sensitivity in the context of heterogeneous tumors.

a. Growth rate of individual clonal allograft tumors. One million clonal cells were injected subcutaneously into the flanks of compatible immune competent mice. Error bars are SEM for n≥3 tumors, * P =0.0155 by t-test for the growth of G8 versus the median rate of the other clones.

b. Schematic depiction of allograft tumor generation using the pooled clonal mixture. One million mixed clonal cells were injected subcutaneously into the flanks of immune competent syngeneic mice.

When tumors had established, the animals were treated with control vehicle, gemcitabine, trametinib, or anti-PD-1 for 2 weeks. Tumors were collected for histology and genomic DNA was isolated.
c. *Trp53*^{R172H} variant allele frequency (VAF) in DNA from ≥5 treated tumors, indicating cancer cell load in the tumors, measured by amplicon deep sequencing of signature mutations. * P =0.0206 t-test VAF in α-PD-1 tumors compared to control tumors. Error bars represent SEM from n=3 sequencing runs for the clonal cell mix, n=4 sequencing runs for control tumors, n=2 sequencing runs for gemcitabine tumors. DNA from ≥5 tumors was pooled per sequencing run.
d – g. VAFs of *Kras*, *Trp53* and 6 genes containing clonal signature mutations, measured by amplicon deep-sequencing, from DNA from (d) the untreated cell mixture and control treated tumors; (e) control and gemcitabine treated tumors; (f) control and trametinib treated tumors; (g) control and α-PD-1 treated tumors. Graphs have a log scale for the y-axes, error bars represent SEM, n=3 deep sequencing runs for the untreated cell mixture, n=5 for the control tumors, n=2 for the gemcitabine and trametinib tumors. DNA from ≥5 tumors was pooled per sequencing run.
h - k. Change in clone abundance in tumors treated with (h) control: (i) gemcitabine; (j) trametinib; or (k) α-PD-1. The graphs have a log scale for the Y-axis; the dashed lines indicate 2-fold increase or decrease in clone abundance. Clone abundance was normalized to total cancer cell load (*Trp53*^{R172H} VAF) in the tumors. Error bars represent SEM, n=5 sequencing repeats for the control tumors, n=2 for the gemcitabine and trametinib tumors. DNA from ≥5 tumors was pooled per sequencing run.

treatment the contribution to tumors was not changed relative to control tumors, whereas a decrease in cancer cell-specific mutant *Trp53*^{R172H} from ~49% to ~38% was observed in the MEK inhibitor treated tumors (Fig. 3c). Although this decrease was not statistically significant, this finding suggests that trametinib may have a greater inhibitory effect on the cancer cells than on the tumor stroma. Strikingly, the α-PD-1 treatment resulted in a significant decrease of mutant *Trp53*^{R172H} DNA to ~14%, compared to ~49% in control tumors (Fig. 3c) due to immune cell recruitment as well as due to cancer cell death. The immune recruitment was validated in the tumor sections, in which showed increased leukocyte infiltration in the α-PD-1 treated tumors (Fig. S4b), whilst the different treatments did not impact the abundance of α-SMA positive fibroblasts (Fig. S4c).

Effects of gemcitabine and trametinib on the growth of clonal subpopulations in heterogeneous tumors are different from the effects in vitro

To monitor clonal drug responses we used deep sequencing of tumor DNA and quantitated the abundance of clonal signature mutations (Table 1). Variant allele frequencies (VAFs) of the clone-specific signature mutations and of mutant *Kras* and *Trp53* under the different treatment conditions are shown in Fig. 3d-g (for absolute read counts see Table S4). Changes in cancer cell subpopulation abundance in the tumors are shown in Fig. 3h-k and discussed in the next sections. Tumor growth of individual clonal tumors without drug treatment revealed the fastest rate for clone G8 and the slowest for C5 and D10 (Fig. 3a). These distinctions were maintained in the heterogeneous tumors (Fig. 3h), indicating that the growth conditions provided in the tumor microenvironment determine clone-specific growth rates.

Next, we compared the impact of gemcitabine and MEK inhibitor treatment on the growth of clonal subpopulations. Only the clone G8 showed a reduced contribution to the tumors after gemcitabine treatment whilst the slow growing clones C5 and D10 gained ~5-fold in abundance (Fig. 3i). Clones C8 and F2, which were inhibited by gemcitabine when grown in the mixed population in vitro (see Fig. 2h) were not impacted by gemcitabine in the heterogeneous tumors in vivo (Fig. 3i). This suggests that the stroma protects clones C8 and F2 from the inhibitory effects of gemcitabine.

The MEK inhibitor treatment of the reconstituted, heterogeneous tumors revealed that clones C8 and G8 are sensitive to trametinib treatment (Fig. 3j), whereas G9 gained in abundance and became the dominant subpopulation in the tumors (Fig. 3f & j). This contrasts with the in vitro findings where clone G9 was sensitive and C8 resistant to trametinib (see Fig. 2j), suggesting that the stroma provides stimuli that alter clonal sensitivity to the MEK inhibitor.

Distinct response of clonal subpopulations in heterogeneous tumors to PD-1 blockade

PDAC is notorious for its dense fibrosis, immune suppressive environment and low number of intratumoral effector T-lymphocytes [48,49]. It has been suggested that these factors drive the low PDAC responsiveness to immune checkpoint inhibition such as anti-programmed death-1 (PD-1) therapy. To assess whether cancer heterogeneity may also play a role in the resistance, we investigated the response of the different clones to anti-PD-1 monoclonal antibody therapy. Similar to the above drug sensitivity assessments, we injected the mixed population of PDAC clones subcutaneously in immune competent mice and treated the animals for 2 weeks. When measuring the clonal contribution to the allograft tumors (Fig. 3g), we found strikingly different responses between the clonal subpopulations. In particular, clone C8 was eliminated after α-PD-1 treatment and clone G9 by >70% (Fig. 3k). Interestingly, the contribution of clones C5 and D10 to the cancer lesions was increased by ~10-fold after the α-PD-1 treatment (Fig. 3k), suggesting that the growth disadvantage of these two clones under control conditions (see Fig. 3h) is not regulated by PD-1 dependent allograft rejection, but due to other microenvironmental factors. The differential clonal sensitivity to leukocyte-mediated killing of clone C8 and G9 initiated by PD-1 blockade suggests cancer cell-intrinsic selectivity and we evaluated the potential mechanism further.

Clonal PDAC cancer cell lines have different abilities to attract leukocytes

Based on the differences in allograft tumor formation and sensitivity to α-PD-1 treatment, we investigated the type of immune cells that infiltrate into the allograft tumors, using flow cytometry (Fig. S5). Analyses of lymphocytes revealed that the highest numbers of infiltrating CD4+ T cells are detected in tumors from clones D10 and G8, whereas the CD8+ T-lymphocytes in the tumors from clones C8, F2 and G9 are higher than in tumors

from the other clones (Fig. 4a). To further elucidate the activation of T-cells in the clonal tumors, we measured CD25 and PD-1 surface expression by flow cytometry. Programmed Cell Death protein-1 (PD-1) is expressed on T-cells upon continuous activation [50]. CD25, also known as Interleukin-2 Receptor α is expressed by regulatory T-cells after stimulation, resulting in CD8+ CD25+ memory T-cells, and CD4+ CD25+ suppressive T-cells [51]. Allograft tumors from clone C8 contain the highest number of CD4+ PD-1+ and CD8+/ PD-1+ that are stimulated via their T-cell receptors (Fig. 4b-c). This might explain the high sensitivity of clone C8 to the α-PD-1 treatment. The second most sensitivity clone to α-PD-1 treatment G9 also has the highest number of tumor infiltration CD8+ PD-1+ T-cells (Fig. 4c), supporting this hypothesis. The number of suppressive CD25+ CD4+ T-cells (mean 36.4% ± 9.1) in the clonal tumors is not associated to different growth phenotypes (Fig. 4b).

Gut associated lymphoid tissue in caecal patches contain cancer reactive T-cells

To investigate whether the differential α-PD-1 sensitivity is mediated by direct cell-cell contact between effector T-lymphocytes and cancer cells, we performed an in vitro co-culture experiment. First, we injected the mixture of the six PDAC clonal cell lines intraperitoneally in immune competent compatible mice to let allograft tumors develop for two weeks. We hypothesized that in tumor bearing mice naïve mouse T-lymphocytes get activated in the gut-associated lymphoid tissue (GALT) such as the Peyer's patches and the caecal patch (the murine equivalent of the human appendix vermiformis [52,53], via their T cell receptor (TCR), mediated by dendritic cells presenting tumor antigens from the cancer cells. Primed T-lymphocytes in the GALT differentiate into effector T-cells, which can migrate to the site of origin of the tumor antigens, and kill the malignant cells [54]. To test this hypothesis we initially studied the histology of the caecal patch lymphoid tissues and found a significant increase in the size of germinal centers in the ceacal patches of tumor bearing KPC mice (Figs. S6a-b), suggesting an increase in immune activation compared to healthy mice.

For functional studies, we subsequently isolated T-lymphocytes from caecal patches of tumor bearing mice for an in vitro activation assay. Figure 4d provides a schematic overview of the procedure. After allowing the mixed clonal allograft tumor growth for two weeks, we isolated T-lymphocytes from the caecal patches of the tumor bearing mice, yielding ~60,000-330,000 live T-cells per mouse. As controls, we isolated T-lymphocytes from the caecal patches of healthy wildtype mice, yielding 45,000-48,000 live T-cells per mouse. Growth media of the T-lymphocytes was supplemented with interleukin-2 (IL-2) and the PDAC clonal cells were added to the cell-cultures. Figure 4e provides a representative view of the PDAC clonal cell mixture growing together with the isolated T-cells after 48 hours. T-cells from healthy mice as well as from tumor bearing mice attach to the PDAC cells (Fig. 4e). Noteably, the PDAC cells in co-culture with T-cells from tumor bearing mice de-attached from the plate at a higher rate and show signs of distress (Fig 4e).

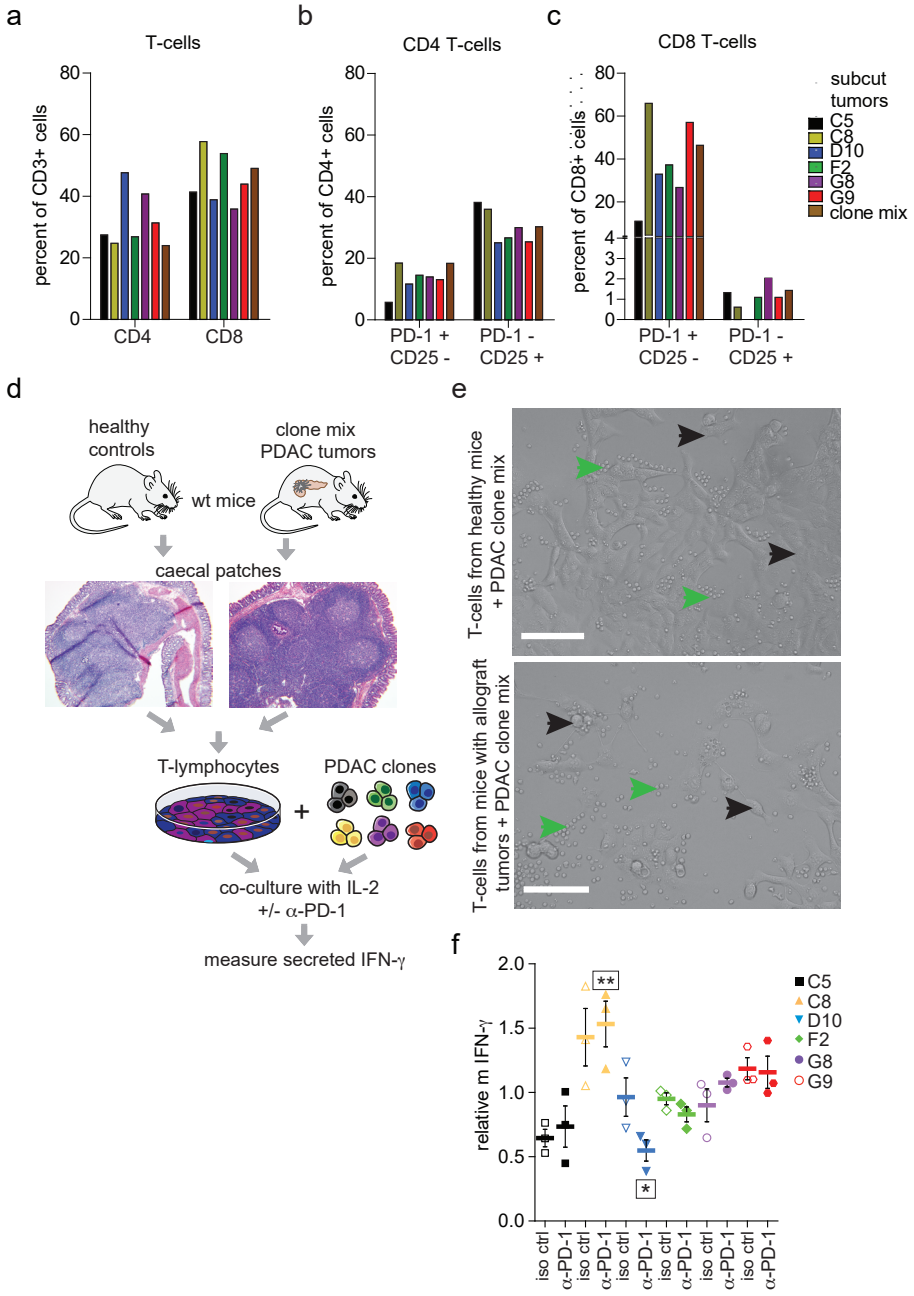

Figure 4. Differential activation of primed T-lymphocytes by clonal pancreatic cancer cells.
a. Flow cytometry results of tumor infiltrating lymphocytes. One million cells of the individual clones, or the clone mixture were injected subcutaneously into the flanks of immune competent syngeneic mice. When tumors had established after 10 days tumors were harvested and processed for flow cytometry analysis. Percentage of CD4 and CD8 T cells are graphed as frequency of total T cells (CD3+ T cells).

b. Flow cytometry results of PD-1 and CD25 expression on CD_4 T cells in allograft tumors.
c. Flow cytometry results of PD-1 and CD25 expression on CD8 T cells in allograft tumors.
d. Schematic of workflow of T-lymphocytes isolation and culture. T-cells were isolated from the caecal patches of healthy control and PDAC allograft tumor bearing mice, and co-cultured together with the PDAC clonal cell lines supplemented with Internleukin-2. After 48 hours, interferon-γ was measured in the supernatants.
e. Images of the PDAC clone mixture and mouse caecal patch T-lymphocytes co-culture in vitro at 48 hours. Green arrows indicate T-lymphocytes, black arrows indicate PDAC cells. Scale bar = 100 μm.
f. Relative amount of IFN-γ in the supernatant of ceacal patch T-lymphocytes from mice that carried clone mix tumors, co-cultured with the individual PDAC clonal cell lines for 48 hours in presence of anti-PD-1 or the igG2a isotype control (iso control), measured by ELISA. Error bars are SEM, measurements from lymphocytes from n=3 mice. Levels of IFN-γ are normalized to the median level of IFN-γ secretion by lymphocytes per mouse. Clone C8 ** P=0.0017 and clone D10 * P = 0.0226, by t-test compared to average level of the other clones.

Clonal cancer cells activate caecal patch T-cells from tumor bearing mice to a different extent

One of the effector mechanisms of activated T-cells is production of Interferon-γ (IFN-γ). Indeed, T-lymphocytes harvested from caecal patches of healthy mice do not secrete IFN-γ when co-cultured with the clonal PDAC cells (Fig. S6b), whereas T-lymphocytes from tumor-bearing mice with intraperitoneal, mixed clone tumors initiated elevated IFN-γ secretion in co-cultures with the clonal PDAC cells (Fig. S6c). Although efficiency of the T-lymphocyte isolation varies between mice (see Fig. S6c), co-cultures of T-cells from tumor bearing mice with PDAC clone C8 elicited the highest level of IFN-γ secretion, and clone G9 the second highest, relative to the other PDAC clones (Fig. 4f). Oncogenic mutation burden and the abundance of tumor infiltrating CD8+ T-lymphocytes are potential predictors for response to anti-PD-1 therapy [55]. Both were found for α-PD-1 sensitive clone C8, which has the highest number of unique non-synonymous mutations (see Fig. 1e-f) and high numbers of tumor infiltration CD8+ T-cells (see Fig. 4a-b). Complementary to these observations, the IFN-γ production by T-cells from allograft tumor bearing mice that are co-cultured with PDAC clone D10 in the presence of α-PD-1 is significantly lower than the levels elicited by the other PDAC clones (Fig. 4d) and this corroborates the resistance of clone D10 to α-PD-1 treatment in vivo (see Fig. 3k). In conclusion, clonal PDAC cell lines originating from the same parental PDAC tumor have distinct intrinsic capacities to activate primed T-lymphocytes in vitro (Fig. 4f), matching with the distinct responses to α-PD-1 treatment in vivo.

We conclude from the above analyses that the crosstalk amongst cancer cell subpopulations and the host stroma impacts the sensitivity to different therapeutic approaches distinctly, allowing the emergence of discrete resistant subpopulations. Moreover, our results suggest that cancer cell-intrinsic factors impact the ab initio sensitivity of subpopulations to immune checkpoint inhibitors.

DISCUSSION

Heterogeneity of human cancers emerges during evolutionary selection of cell subpopulations with different genetic and epigenetic alterations that provide a survival advantage under pressure from the microenvironment [9,10,13,26] and continues during therapy [17]. Crosstalk between tumor subpopulations is one of the modulators that impact cell growth and was recognized in a mammary tumor model several decades ago [56]. A recent study systematically evaluated and modeled this crosstalk via secreted factors [28]. The authors used the established human breast cancer cell line MDA-MB-468 to generate a panel of eighteen derivative cell lines by lentiviral expression of single secreted factors and showed that paracrine stimuli from small, less fit clonal subpopulations can still drive malignant progression of xenograft tumors in immune-compromised mice. Also, the biologic significance of a highly dynamic but small subpopulation of cells was uncovered in human melanoma. It was shown that epigenetic regulation by an H3K4 demethylase maintains a slow growing, minor subpopulation in melanoma that can escape from treatments targeting fast growing populations, can repopulate the tumor and contribute to metastatic growth [57]. Patient derived xenografts (PDXs) can partially retain tumor heterogeneity [58]. However, PDXs need to be maintained in immune compromised animals and thus retain only a subset of the microenvironmental features. These examples illustrate the complex biology and challenges to generate appropriate experimental platforms that capture the dynamics of tumor evolution and allow for the assessment of therapeutic interventions.

In this study, we first deconvoluted a PDAC tumor from the classic KPC model into clonal cell lines and then reconstituted heterogeneous tumors to follow clonal dynamics during drug treatment in syngeneic, immune competent hosts. Based on the signature mutations identified for each clone and the shared *Trp53* variant allele amongst the clones, the relative abundance and stromal contribution can be quantitated in our model in the context of an intact immune environment. One of our findings was that clonal cell growth of the mixed population in vitro correlated only in part with growth in the presence of host stroma and immune cells. Under control conditions the growth in vivo of some clones was slower despite their indistinguishable growth rates in vitro. This suggests that the crosstalk with immune cells and tumor stroma is different for these clonal cancer cells, though they were derived from the same original tumor specimen.

Previous studies have shown the impact of stromal signals on cancer cell drug sensitivity [59,60] and more recent models have tried to capture some of the features of the environment in vitro [59-63]. In the current study, the MEK kinase inhibitor showed the most striking differences between the findings in vitro and in vivo and we attribute some of this to the impact of the inhibitor on crosstalk between cancer cells and stromal cells. Paracrine clonal

crosstalk amongs cancer cells can explain the sensitization of clone G8 that was resistant to trametinib on its own but sensitized in the mixed cancer cell culture in vitro. A comparison of clonal effects of trametinib in the mixed culture in vitro and in the tumors however, showed a discordant result for clone G9 that moved from sensitive in vitro to resistant in the tumors and clone C8 that moved in the opposite direction (see Fig. 2j vs Fig. 3j). Still, under the MEK inhibitor treatment stromal cell abundance increased (Fig. 3c) suggesting additional crosstalk of tumor cells and stroma that altered the clonal sensitivity in vivo.

The potential contribution of host immune cells to the differential growth we observed in vivo versus in vitro is suggested by earlier studies. One classic study showed distinct immunogenicity of clonal subpopulations of a mouse mammary adenocarcinoma [64]. Surprisingly, we found that immune checkpoint blockade, which leads to increased lymphocyte-mediated cancer cell killing [65,66], did not reduce the growth of slow growing clones any further. In contrast, these clones increased in abundance in the residual tumor after α-PD-1 treatment and thus appear resistant to checkpoint inhibition. Also, the slower clones C5 and D10 increased in abundance after treatment with the cytotoxic drug gemcitabine. This finding is reminiscent of a recent report that showed that minor dormant human colorectal cancer clones can become dominant and reinitiate tumor growth after chemotherapy [67].

The striking differences in immunotherapy efficacy towards clones present in heterogeneous tumor mix provides some interesting insights that may allow to overcome resistance. One of the clonal cell lines, clone C8, is particularly sensitive to α-PD-1 therapy. The co-culture experiment with primed mouse T-lymphocytes and the clonal PDAC cell lines corroborated the finding. Antigens specific to clone C8 activated primed T-lymphocytes significantly better than those of the other clonal lines generated from the same tumor. TILs are often exhausted and thus difficult to use in cell culture experiments [68]. We conducted this experiment with T-lymphocytes from the caecal patches of allograft tumor bearing mice. We are the first to show that caecal patches of in PDAC bearing mice contain cancer-specific effector T-cells, providing a new approach to assess immunotherapy efficacy.

In conclusion, the composition of heterogeneous cancers is affected by crosstalk amongst the cancer subpopulations as well as the host environment that includes the immune system as a major player. We developed an in vivo model that allows for the quantitation of clonal cancer subpopulations in heterogeneous tumors, growing in immune competent animals. Our model is suited for the assessment of stromal and immune modulators and their impact on growth of heterogeneous cancer cells. Our study shows that prediction of drug efficacy from in vitro analysis of heterogeneous cancer cell populations is dependent on the mechanism of action of the studies drugs. Immune response and sensitivity to checkpoint

blockade is cancer clone specific and predictable using co-cultures with appropriately primed effector T-cells.

Data availability statement

The RNA and exome sequencing datasets generated during the current study are available from the corresponding author on reasonable request.

Acknowledgements

The authors thank Dr. Bhaskar Kallakury for his histopathology consultation, Jeroen Versteeg and Cristoforo Grasso for assistance in tissue collection and processing and Dr. Robert Beckman for critical reading of the manuscript. The work was supported by grants from the NIH/NCI CA51008 (AW), CA71508 (AW), CA113477 (ATR), CA177466 (AW). Additional support was from the Intramural Research Program of the National Institutes of Health, National Cancer Institute, Center for Cancer Research.

Author contributions

EEV, AW and ATR conceived the project and generated the manuscript. IP and EEV generated the clonal cell lines. EBB performed the 3D matrix cell cultures, and edits to the manuscript. EBB and EEV performed the analysis of the exome sequencing data. MDP and MOS performed the RNA seq analysis. EEV, SMR, AJ, MDP, IP and MHBCS performed animal studies and tumor analyses. JKS designed the in vitro drug assays and clonal drug sensitivity. EEV, JKS and MHBCS performed the in vitro drug screens**.** EEV, AJ and SMR performed the ddPCR, qPCR and amplicon experiments**.** JNM and EEV performed amplicon deep sequencing and analysis**.** SMR, MM and MC performed the flow cytometry analyses. BAM and ATR contributed to advancements of the project and edits of the manuscript. All authors discussed and approved the manuscript.

Competing financial interests and Conflicts of interest

The authors have no competing financial interests or conflicts of interest to disclose.

Supplementary Table 1. List of ubiquitous non-synonymous single nucleotide variations in the clonal cancer cell lines and the corresponding parental tumor tissue measured by exome sequencing.
AAS = amino acid substitution

Gene	AAS	Gene	AAS	Gene	AAS	Gene	AAS
AB124611	D73G	*Kri1*	K241E	*Rbm12b2*	T574P	*Tmem52*	T91P
Aloxe3	A667V	*Lzts2*	H327Q	*Rbpjl*	T368S	*Tonsl*	T1086M
Atp13a4	F568L	*Mbp*	G27R	*Sec16b*	R31C	*Trp53*	R172H
Car4	A97V	*Ncoa3*	A706V	*Shisa6*	L368I	*Trp53rkb*	A208E
Clec2g	N12S	*Nfam1*	R220S	*Slc15a5*	G452S	*Ttll8*	R702L
Cntn5	T966A	*Nrip2*	P158S	*Slc30a4*	G64R	*Ugt1a1*	K80M
Cox11	V62A	*Nup160*	L7R	*Slc45a1*	S433L	*Uimc1*	E709D
Cypt4	N152S	*Olfr311*	A210T	*Slfn14*	V301I	*Vmn1r12*	F61L
Dock6	W145R	*Olfr314*	T238A	*Smco2*	T163N	*Vmn1r15*	T38I
Ecsit	S75L	*Olfr743*	N84S	*Smco3*	K193R	*Vmn1r6*	L264V
Gjd4	V80L	*Pdcd11*	P1556L	*Spint3*	T86I	*Wbp11*	D360N
Gm14459	M80I	*Pitpnm3*	R21Q	*Srebf2*	R621H	*Wfdc12*	L70P
Gtse1	P399L	*Ppfibp1*	L371P	*Tas2r136*	G202D	*Xaf1*	C135S
Kcnk15	I195V	*Ppl*	G179R	*Tekt1*	A237V	*Yipf2*	L227F
Klrc2	A188P	*Rangap1*	E389D	*Timm9*	R89W	*Zc3h7b*	A681T
Kras	G12D	*Rbbp8*	K178R	*Tmem241*	A85S	*Zfp426*	S54T

Supplementary Table 2. Unique signature single nucleotide variations in the clonal cell lines and the parental tumor measured by exome sequencing. Mutations in bold are used as clone identifiers in the heterogeneous mixtures.

Clone C5	Clone C8	Clone D10	Clone F2	Clone G8	Clone G9	Parental tumor tissue
***Baiap3*,L170I**	*1700113H08Rik*, I192S	*4921524L21Rik*,	*AA792892*, K124N	*4933402J07Rik*,K17M	*Ctnna3*,L211V	*4933409G03Rik*,
Btnl2,A244V	*Abcc12*,S895G	Q233H	*Abca1*,F1535V	*Adad2*,T459P	*Ctsm*,R109H	D188E
Ceacam1, V437G	*Adrbk1*,P679A	*4930444G20Rik*,	*Bcor*,T941P	***Arhgap25*,**	*Cybrd1*,H188R	*A830010M20Rik*,P47T
Epn1,T347P	*Apoc2*,L68F	H69Q	*Ccdc61*,A5P	**K171R**	*Frmpd3*,M429V	*C2cd4a*,R284C
Flg2,Q1327P	*Apol7b*,L353P	*Adh4*,I374T	*Ccr1*,S191T	*Bmper*,T570P	*Grin2d*,A764G	*Ceacam20*,S470N
Ifit2,D207E	*Atpaf1*,K267N	*Anapc5*,A522V	*Cln3*,I286T	*Creld2*,A44G	*Hnf4a*,R177W	*Cep290*,M2352L
Ifna7,R60G	*Bcorl1*,A242G	*Cgn*,Q1077H	*Hapln4*,L67F	*Dennd1c*,T495P	*Hyou1*,S527R	*Cux1*,L1583P
Jak3,D809A	*Cdh11*,R137K	*Chd6*,A1204G	*Herc3*,N424S	*Depdc7*,M103I	*Ighmbp2*,K866N	*Dcpp3*,T39A
L3mbtl1,A146V	*Cdk4*,D221H	*Cldn4*,V32G	*Huwe1*,T3219P	*Gpr89*,V336G	*Ino80*,A1457P	*Defa34*,K24N
Ocm,A41P	*Cfh*,L138P	*Coa7*,V41G	*Llgl2*,T247P	*H2-T9*,H167Q	*Lrp12*,V671G	*Dpy19l1*,L367V
Olfr1212,L65P	*Clpsl2*,D92A	*Coro6*,I50V	*Lrp2*,I3348M	*Mafk*,K141T	*Mmrn1*,T389M	*Duox1*,H129R
Olfr1214, A118S	*Crb2*,L655F	*Elf4*,S496I	***Matn4*,R339Q**	*Pcdhga12*,	*Mnda*,S205L	*Dyrk1b*,D668A
Slc24a3,T291P	*Csf2rb*,K195N	*Gtf2a2*,A33V	*Olfr368*,C183Y	A696P	*Nlrp1a*,S827T	*Ear10*,T30P
Snx14,G7R	*Cyp2c54*,K399T	*Klhl13*,Q416H	*Pcdhgb8*,	*Ppp1r10*,C463R	*Nudt12*,H251P	*Fhad1*,T1129M
Snx33,H140P	*Dagla*,A777P	*Lactbl1*,S317A	S170R	*Rnf121*,T119P	***Pla2g4d*,S710R**	*Gm14085*,V338F
Spata31d1c, T688A	*Dctn1*,R1236K	*Maneal*,V216G	*Psg18*,L259I	*Siglech*,H79P	*Plp2*,F78L	*Gm4303*,Q253H
Tacc2,T2575P	*Dlgap4*,A962P	*Mark4*,L469F	*Psg27*,F151I	*Tcf25*,E512D	*Prg4*,T441P	*Hic1*,S23P
Vmn1r193,	*Dmd*,G3185E	*Mcm9*,K38N	*Ptgis*,P489A	*Tnk2*,D471A	*Pydc4*,E91V	*Itgad*,P1119L
I156V	*Fat4*,T3878P	***Nox4*,T163M**	*Rapgefl1*,	*Usp49*,A13P	*Rapgef4*,N213S	*Kank3*,R165G
	Fbln5,Y66D	*Nup155*,V280F	A429G	*Vmn2r84*,R571T	*Rars2*,T466P	*Kazn*,G48R
	Fbxw19,L212S	*Pmaip1*,L94F	*Rrs1*,L218M		*Ret*,R960P	*Lactbl1*,S539A
	Fcgr2b,T66I	*Rgl2*,D216A	*Slc22a20*,		*Sparcl1*,D199E	*Macrod2*,K6N
	Fgfr3,G650D	*Tle3*,S407C	L472F		*Tas2r134*,C50F	*Mrps35*,T11S
	Fmo2,H154P	*Tyk2*,T865P	*Slc6a3*,R614C		*Ubr4*,Q3355K	*Naf1*,L187P

Supplementary Table 2. Unique signature single nucleotide variations in the clonal cell lines and the parental tumor measured by exome sequencing. Mutations in bold are used as clone identifiers in the heterogeneous mixtures. (continued)

Clone C5	Clone C8	Clone D10	Clone F2	Clone G8	Clone G9	Parental tumor tissue
	Gm12171,H57R	*Vmn1r20*,S94T	*Sulf1*,L607F		*Zfp663*,E35D	*Olfr221*,R303K
	Gm13083,A18V	*Zfp458*,E469G	*Tert*,F550L			*Olfr311*,M101I
	Gm13271, S176Y					*Olfr311*,V96A
	Gnas,D962Y					*Pdzd3*,T10K
	H2-M10.1, P234L					*Phyh*,Y46F
	H2-M10.5, N245I					*Pira6*,G199S
	Hydin,T4349P					*Pkd1*,L3P
	Ifna9,S81T					*Prkag2*,V229A
	Kcna5,G127A					*Prr3*,G27V
	Kcnc2,T366P					*Rsf1*,A4T
	Klhl36,D369A					*Samd8*,S15Y
	Laptm5,L121V					*Sap130*,T992N
	Map2,A831G					*Sbpl*,S135N
	Masp2,G528D					*Smyd1*,V114G
	Megf8,C612W					*Tgds*,G133R
	Mier3,R311W					*Tgs1*,V323L
	Mmp16,D400H					*Tmc1*,A372G
	Myh2,I1032T					*Ube2ql1*,S48G
	Myh7,E981K					*Vmn1r124*,T289P
	Nlrc3,V1100L					*Zcchc3*,T63A
	Olfml3,A195S					*Zkscan4*,T109A
	Olfr113,A95G					
	***Olfr1157*,I289M**					
	Olfr1511,A165T					

Supplementary Table 2. Unique signature single nucleotide variations in the clonal cell lines and the parental tumor measured by exome sequencing. Mutations in bold are used as clone identifiers in the heterogeneous mixtures. (continued)

Clone C5	Clone C8	Clone D10	Clone F2	Clone G8	Clone G9	Parental tumor tissue
	Olfr175-ps1, N89D					
	Olfr312,Q136H					
	Olfr661,S10N					
	Olfr742,I37V					
	Osgep,E330D					
	Pcdhb4,R624H					
	Pde3b,R223K					
	Pdf,P171R					
	Phf8,C327W					
	Sec24c,S26W					
	Serpina3i,S81G					
	Sfi1,E1110K					
	Sidt1,H24R					
	Slc15a4,E433G					
	Slc25a3,V5I					
	Slc26a10,S279T					
	Sorbs3,P678L					
	Sp140,S461G					
	Spsb2,A72G					
	Tbc1d16,A325P					
	Tcf7l1,E62K					
	Tmem132e, V176A					
	Tmem232, A273T					
	Tnc,Q149H					

Supplementary Table 2. Unique signature single nucleotide variations in the clonal cell lines and the parental tumor measured by exome sequencing. Mutations in bold are used as clone identifiers in the heterogeneous mixtures. (continued)

Clone C5	Clone C8	Clone D10	Clone F2	Clone G8	Clone G9	Parental tumor tissue
	Tubb4b,G140V					
	Ubap2,Y941H					
	Usp19,L805V					
	Vmn1r171,I30V					
	Vmn1r205, I188M					
	Vmn1r9,S108N					
	Vmn2r104, N611H					
	Vmn2r115, D500G					
	Vmn2r28,C756F					
	Vmn2r49,E40G					
	Vmn2r52,R690K					
	Vmn2r60,F777L					
	Vmn2r78,T257I					
	Vps13c,T2230A					
	Wbscr27,R88P					
	Zfp874b,R297M					
	Zfp982,V100I					

Supplementary Table 3. Deep sequencing read counts of the clone-specific signature mutations and ubiquitous *Kras* and *Trp53* mutations in DNA from the heterogeneous clone mixtures in vitro. chrom = chromosome; mm9 = mus musculus reference genome 9; VAF = variant allele frequency

EQUAL MIX OF UNTREATED CLONAL CELLS – DEEP-SEQ RUN 1								
clone	**gene**	**chrom**	**position (mm9)**	**variant**	**read depth**	**wildtype reads**	**variant reads**	**VAF**
all	*Trp53*	chr11	69402014	G>A	NA	NA	NA	NA
all	*Kras*	chr6	145195291	C>T	725	264	461	63.59%
C5	*Baiap3*	chr17	25387359	G>T	1235	1203	32	2.59%
C8	*Olfr1157*	chr2	87802181	G>C	501	475	26	5.19%
D10	*Nox4*	chr7	94462586	C>T	651	625	26	3.99%
F2	*Matn4*	chr2	164222680	C>T	508	475	33	6.50%
G8	*Arhgap25*	chr6	87426299	T>C	1207	1136	71	5.88%
G9	*Pla2g4d*	chr2	120094626	G>T	656	583	73	11.13%

EQUAL MIX OF UNTREATED CLONAL CELLS – DEEP-SEQ RUN 2								
clone	**gene**	**chrom**	**position (mm9)**	**variant**	**read depth**	**wildtype reads**	**variant reads**	**VAF**
all	*Trp53*	chr11	69402014	G>A	860	0	855	99.42%
all	*Kras*	chr6	145195291	C>T	533	184	349	65.48%
C5	*Baiap3*	chr17	25387359	G>T	1298	1264	34	2.62%
C8	*Olfr1157*	chr2	87802181	G>C	825	797	28	3.39%
D10	*Nox4*	chr7	94462586	C>T	955	883	72	7.54%
F2	*Matn4*	chr2	164222680	C>T	1050	925	125	11.90%
G8	*Arhgap25*	chr6	87426299	T>C	1230	1141	87	7.07%
G9	*Pla2g4d*	chr2	120094626	G>T	742	704	38	5.12%

EQUAL MIX OF UNTREATED CLONAL CELLS – DEEP-SEQ RUN 3								
clone	**gene**	**chrom**	**position (mm9)**	**variant**	**read depth**	**wildtype reads**	**variant reads**	**VAF**
all	*Trp53*	chr11	69402014	G>A	2371	20	2331	98.31%
all	*Kras*	chr6	145195291	C>T	2575	1012	1562	60.66%
C5	*Baiap3*	chr17	25387359	G>T	2651	2531	120	4.53%
C8	*Olfr1157*	chr2	87802181	G>C	2663	2522	140	5.26%
D10	*Nox4*	chr7	94462586	C>T	2823	2643	180	6.38%
F2	*Matn4*	chr2	164222680	C>T	2614	2381	232	8.88%
G8	*Arhgap25*	chr6	87426299	T>C	3340	3177	157	4.70%
G9	*Pla2g4d*	chr2	120094626	G>T	2370	2027	336	14.18%

MIX OF CELLS GROWN IN VITRO WITH DMSO – DEEP-SEQ RUN 1								
clone	**gene**	**chrom**	**position (mm9)**	**variant**	**read depth**	**wildtype reads**	**variant reads**	**VAF**
all	*Trp53*	chr11	69402014	G>A	1415	0	1407	99.43%
all	*Kras*	chr6	145195291	C>T	1247	434	813	65.20%
C5	*Baiap3*	chr17	25387359	G>T	1492	1461	31	2.08%
C8	*Olfr1157*	chr2	87802181	G>C	0	-	-	-
D10	*Nox4*	chr7	94462586	C>T	2011	1930	81	4.03%
F2	*Matn4*	chr2	164222680	C>T	0	-	-	-
G8	*Arhgap25*	chr6	87426299	T>C	2551	2413	137	5.37%
G9	*Pla2g4d*	chr2	120094626	G>T	1658	1499	159	9.59%

MIX OF CELLS GROWN IN VITRO WITH DMSO – DEEP-SEQ RUN 2								
clone	**gene**	**chrom**	**position (mm9)**	**variant**	**read depth**	**wildtype reads**	**variant reads**	**VAF**
all	*Trp53*	chr11	69402014	G>A	2054	6	2027	98.69%
all	*Kras*	chr6	145195291	C>T	2578	1056	1522	59.04%
C5	*Baiap3*	chr17	25387359	G>T	2439	2385	53	2.17%
C8	*Olfr1157*	chr2	87802181	G>C	3013	2770	243	8.07%
D10	*Nox4*	chr7	94462586	C>T	2868	2705	163	5.68%
F2	*Matn4*	chr2	164222680	C>T	2795	2393	398	14.24%
G8	*Arhgap25*	chr6	87426299	T>C	3566	3319	246	6.90%
G9	*Pla2g4d*	chr2	120094626	G>T	2448	2199	244	9.97%

MIX OF CELLS GROWN IN VITRO WITH GEMCITABINE – DEEP-SEQ RUN 1								
clone	**gene**	**chrom**	**position (mm9)**	**variant**	**read depth**	**wildtype reads**	**variant reads**	**VAF**
all	*Trp53*	chr11	69402014	G>A	1227	0	1221	99.51%
all	*Kras*	chr6	145195291	C>T	858	294	564	65.73%
C5	*Baiap3*	chr17	25387359	G>T	1891	1812	79	4.18%
C8	*Olfr1157*	chr2	87802181	G>C	1405	1392	13	0.93%
D10	*Nox4*	chr7	94462586	C>T	924	851	73	7.90%
F2	*Matn4*	chr2	164222680	C>T	1620	1591	29	1.79%
G8	*Arhgap25*	chr6	87426299	T>C	1663	1634	29	1.74%
G9	*Pla2g4d*	chr2	120094626	G>T	1316	845	469	35.64%

MIX OF CELLS GROWN IN VITRO WITH TRAMETINIB– DEEP-SEQ RUN 1								
clone	**gene**	**chrom**	**position (mm9)**	**variant**	**read depth**	**wildtype reads**	**variant reads**	**VAF**
all	*Trp53*	chr11	69402014	G>A	869	1	866	99.65%
all	*Kras*	chr6	145195291	C>T	740	256	484	65.41%
C5	*Baiap3*	chr17	25387359	G>T	948	933	14	1.48%
C8	*Olfr1157*	chr2	87802181	G>C	805	680	125	15.53%
D10	*Nox4*	chr7	94462586	C>T	1022	1016	6	0.59%
F2	*Matn4*	chr2	164222680	C>T	940	853	87	9.26%
G8	*Arhgap25*	chr6	87426299	T>C	1555	1439	114	7.33%
G9	*Pla2g4d*	chr2	120094626	G>T	843	831	12	1.42%

Supplementary Table 4. Deep sequencing read counts of the clone-specific mutations and ubiquitous *Kras* and *Trp53* mutations in DNA from the heterogeneous allograft tumors after 2 weeks treatment. chrom = chromosome; mm9 = mus musculus reference genome 9; VAF = variant allele frequency; * = Arbitrary number, set as minimum sequencing detection threshold (in the case of 0 mutant reads).

SUBCUT TUMORS AFTER CONTROL TREATMENT – DEEP-SEQ RUN 1								
clone	**gene**	**chrom**	**position (mm9)**	**variant**	**read depth**	**wildtype reads**	**variant reads**	**VAF**
all	*Trp53*	chr11	69402014	G>A	0	-	-	-
all	*Kras*	chr6	145195291	C>T	474	387	87	18.35%
C5	*Baiap3*	chr17	25387359	G>T	1519	1519	0	0.01% *
C8	*Olfr1157*	chr2	87802181	G>C	430	418	12	2.79%
D10	*Nox4*	chr7	94462586	C>T	567	567	0	0.01% *
F2	*Matn4*	chr2	164222680	C>T	1038	1009	29	2.79%
G8	*Arhgap25*	chr6	87426299	T>C	1120	1073	47	4.19%
G9	*Pla2g4d*	chr2	120094626	G>T	782	755	27	3.45%

SUBCUT TUMORS AFTER CONTROL TREATMENT – DEEP-SEQ RUN 2								
clone	**gene**	**chrom**	**position (mm9)**	**variant**	**read depth**	**wildtype reads**	**variant reads**	**VAF**
all	*Trp53*	chr11	69402014	G>A	854	471	379	44.38%
all	*Kras*	chr6	145195291	C>T	760	502	258	33.95%
C5	*Baiap3*	chr17	25387359	G>T	948	948	0	0.01% *
C8	*Olfr1157*	chr2	87802181	G>C	829	806	23	2.77%
D10	*Nox4*	chr7	94462586	C>T	1060	1057	3	0.28%
F2	*Matn4*	chr2	164222680	C>T	1981	1782	196	9.89%
G8	*Arhgap25*	chr6	87426299	T>C	1236	1192	44	3.56%
G9	*Pla2g4d*	chr2	120094626	G>T	943	890	52	5.51%

SUBCUT TUMORS AFTER CONTROL TREATMENT – DEEP-SEQ RUN 3								
clone	**gene**	**chrom**	**position (mm9)**	**variant**	**read depth**	**wildtype reads**	**variant reads**	**VAF**
all	*Trp53*	chr11	69402014	G>A	588	419	168	28.57%
all	*Kras*	chr6	145195291	C>T	953	658	294	30.85%
C5	*Baiap3*	chr17	25387359	G>T	1303	1300	2	0.15%
C8	*Olfr1157*	chr2	87802181	G>C	923	921	2	0.22%
D10	*Nox4*	chr7	94462586	C>T	1138	1135	1	0.09%
F2	*Matn4*	chr2	164222680	C>T	1120	1106	13	1.16%
G8	*Arhgap25*	chr6	87426299	T>C	1202	1145	57	4.74%
G9	*Pla2g4d*	chr2	120094626	G>T	1196	1194	2	0.17%

SUBCUT TUMORS AFTER CONTROL TREATMENT – DEEP-SEQ RUN 4								
clone	**gene**	**chrom**	**position (mm9)**	**variant**	**read depth**	**wildtype reads**	**variant reads**	**VAF**
all	*Trp53*	chr11	69402014	G>A	4074	1614	2431	59.67%
all	*Kras*	chr6	145195291	C>T	5669	4354	1314	23.18%
C5	*Baiap3*	chr17	25387359	G>T	5280	5256	20	0.38%
C8	*Olfr1157*	chr2	87802181	G>C	5823	5732	87	1.49%
D10	*Nox4*	chr7	94462586	C>T	5705	5691	13	0.23%
F2	*Matn4*	chr2	164222680	C>T	3889	3551	336	8.64%
G8	*Arhgap25*	chr6	87426299	T>C	6124	5833	284	4.64%
G9	*Pla2g4d*	chr2	120094626	G>T	5286	4538	742	14.04%

SUBCUT TUMORS AFTER CONTROL TREATMENT – DEEP-SEQ RUN 5								
clone	**gene**	**chrom**	**position (mm9)**	**variant**	**read depth**	**wildtype reads**	**variant reads**	**VAF**
all	*Trp53*	chr11	69402014	G>A	2638	985	1635	61.98%
all	*Kras*	chr6	145195291	C>T	4076	2355	1721	42.22%
C5	*Baiap3*	chr17	25387359	G>T	4422	4411	11	0.25%
C8	*Olfr1157*	chr2	87802181	G>C	5481	5282	197	3.59%
D10	*Nox4*	chr7	94462586	C>T	4177	4172	5	0.12%
F2	*Matn4*	chr2	164222680	C>T	4668	4194	470	10.07%
G8	*Arhgap25*	chr6	87426299	T>C	5218	4891	326	6.25%
G9	*Pla2g4d*	chr2	120094626	G>T	4372	4193	170	3.89%

SUBCUT TUMORS AFTER GEMCITABINE TREATMENT – DEEP-SEQ RUN 1								
clone	**gene**	**chrom**	**position (mm9)**	**variant**	**read depth**	**wildtype reads**	**variant reads**	**VAF**
all	*Trp53*	chr11	69402014	G>A	1142	487	645	56.48%
all	*Kras*	chr6	145195291	C>T	1329	844	485	36.49%
C5	*Baiap3*	chr17	25387359	G>T	1625	1613	12	0.74%
C8	*Olfr1157*	chr2	87802181	G>C	1241	1200	39	3.14%
D10	*Nox4*	chr7	94462586	C>T	1467	1451	16	1.09%
F2	*Matn4*	chr2	164222680	C>T	1644	1510	134	8.15%
G8	*Arhgap25*	chr6	87426299	T>C	1784	1740	44	2.47%
G9	*Pla2g4d*	chr2	120094626	G>T	1453	1380	73	5.02%

SUBCUT TUMORS AFTER GEMCITABINE TREATMENT – DEEP-SEQ RUN 2								
clone	**gene**	**chrom**	**position (mm9)**	**variant**	**read depth**	**wildtype reads**	**variant reads**	**VAF**
all	*Trp53*	chr11	69402014	G>A	1923	1159	751	39.05%
all	*Kras*	chr6	145195291	C>T	3141	2795	345	10.98%
C5	*Baiap3*	chr17	25387359	G>T	2539	2525	13	0.51%
C8	*Olfr1157*	chr2	87802181	G>C	3644	3601	39	1.07%
D10	*Nox4*	chr7	94462586	C>T	3444	3432	11	0.32%
F2	*Matn4*	chr2	164222680	C>T	3050	2895	154	5.05%
G8	*Arhgap25*	chr6	87426299	T>C	3536	3494	40	1.13%
G9	*Pla2g4d*	chr2	120094626	G>T	2951	2796	152	5.15%

SUBCUT TUMORS AFTER TRAMETINIB TREATMENT – DEEP-SEQ RUN 1								
clone	**gene**	**chrom**	**position (mm9)**	**variant**	**read depth**	**wildtype reads**	**variant reads**	**VAF**
all	*Trp53*	chr11	69402014	G>A	-	-	-	-
all	*Kras*	chr6	145195291	C>T	1195	955	240	20.08%
C5	*Baiap3*	chr17	25387359	G>T	1883	1882	1	0.05%
C8	*Olfr1157*	chr2	87802181	G>C	884	880	4	0.45%
D10	*Nox4*	chr7	94462586	C>T	1105	1104	1	0.09%
F2	*Matn4*	chr2	164222680	C>T	1293	1259	34	2.63%
G8	*Arhgap25*	chr6	87426299	T>C	2013	1982	31	1.54%
G9	*Pla2g4d*	chr2	120094626	G>T	1147	1037	110	9.59%

SUBCUT TUMORS AFTER TRAMETINIB TREATMENT – DEEP-SEQ RUN 2								
clone	**gene**	**chrom**	**position (mm9)**	**variant**	**read depth**	**wildtype reads**	**variant reads**	**VAF**
all	*Trp53*	chr11	69402014	G>A	2199	1361	833	37.88%
all	*Kras*	chr6	145195291	C>T	3242	2397	845	26.06%
C5	*Baiap3*	chr17	25387359	G>T	2275	2269	6	0.26%
C8	*Olfr1157*	chr2	87802181	G>C	3813	3795	16	0.42%
D10	*Nox4*	chr7	94462586	C>T	2563	2559	2	0.08%
F2	*Matn4*	chr2	164222680	C>T	2634	2494	137	5.20%
G8	*Arhgap25*	chr6	87426299	T>C	3467	3425	41	1.18%
G9	*Pla2g4d*	chr2	120094626	G>T	3068	2647	417	13.59%

SUBCUT TUMORS AFTER α-PD-1 TREATMENT – DEEP-SEQ RUN 1								
clone	**gene**	**chrom**	**position (mm9)**	**variant**	**read depth**	**wildtype reads**	**variant reads**	**VAF**
all	*Trp53*	chr11	69402014	G>A	497	428	69	13.88%
all	*Kras*	chr6	145195291	C>T	594	561	33	5.56%
C5	*Baiap3*	chr17	25387359	G>T	639	636	3	0.47%
C8	*Olfr1157*	chr2	87802181	G>C	455	455	0	0.01% *
D10	*Nox4*	chr7	94462586	C>T	682	678	4	0.59%
F2	*Matn4*	chr2	164222680	C>T	638	632	6	0.94%
G8	*Arhgap25*	chr6	87426299	T>C	754	740	13	1.72%
G9	*Pla2g4d*	chr2	120094626	G>T	519	517	2	0.39%

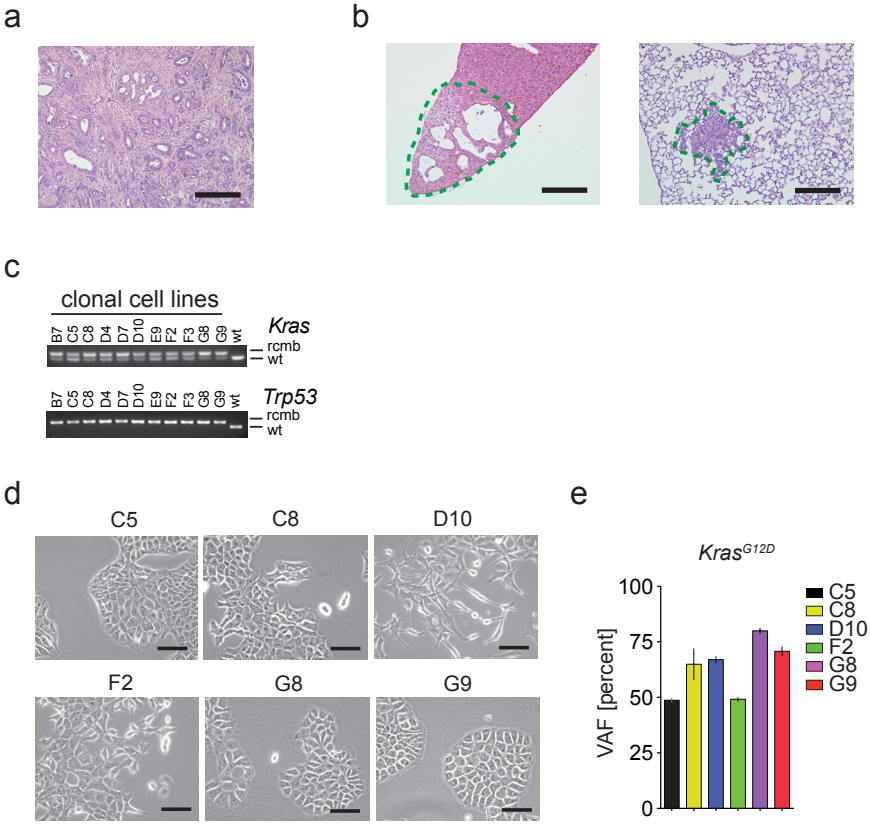

Supplementary Figure 1. Characterization of heterogeneous clonal cell lines from a KPC mouse pancreatic tumor (Related to Figure 1)

a, b. Images of H&E stained, formalin fixed paraffin embedded (FFPE) primary KPC mouse pancreatic tumor (a) as well as liver and lung metastases (b). Scale bar = 100 μm.

c. Allele specific PCR products of *Kras* and *Trp53* DNA from eleven clonal KPC PDAC cell lines that underwent Cre recombination. Lower bands indicate wildtype (wt) alleles; upper bands are the recombined alleles containing the 34 basepair LoxP.

d. Images taken from the 2D monolayers of the individual clonal cell lines in vitro. Scale bar = 30 μm.

e. $Kras^{G12D}$ variant allele frequency (VAF) in six clonal cell lines. Droplet Digital PCR was performed using a HEX labeled probe for wildtype *Kras* and a FAM labeled probe for mutant $Kras^{G12D}$. Data is presented as ratio of positive $Kras^{G12D}$ droplets over total *Kras* positive droplets is shown. Error bars are SEM of 2 replicate PCR reactions from 2 clonal cell DNA preparations.

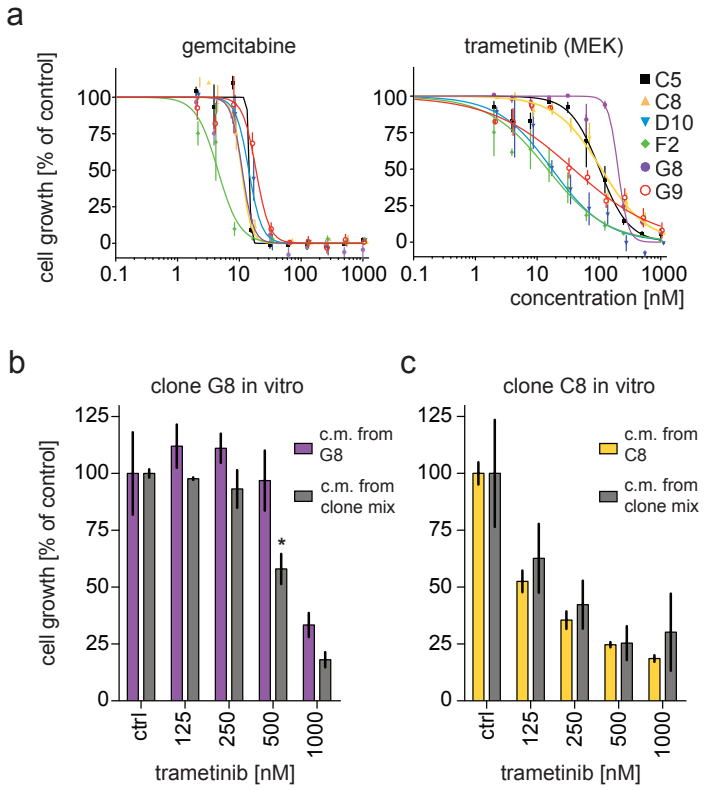

Supplementary Figure 2. Distinct clonal growth rates and drug sensitivity (Related to Figure 2)
a. Dose response curves of gemcitabine or trametinib after 72 hours. Drugs were added to the clonal PDAC cell lines one day after plating. Error bars are SEM from triplicate wells.
b, c. Dose-response of trametinib for clone G8 (b) and C8 (c) in the presence of conditioned media (c.m.) harvested from the clone mixture or from G8 or C8 only. A 1:1 ratio of c.m. and DMEM/10%FBS was used. Error bars are SEM of 2 replicate experiments, * p< 0.05 t-test for c.m. from the clone mix vs c.m. from G8.

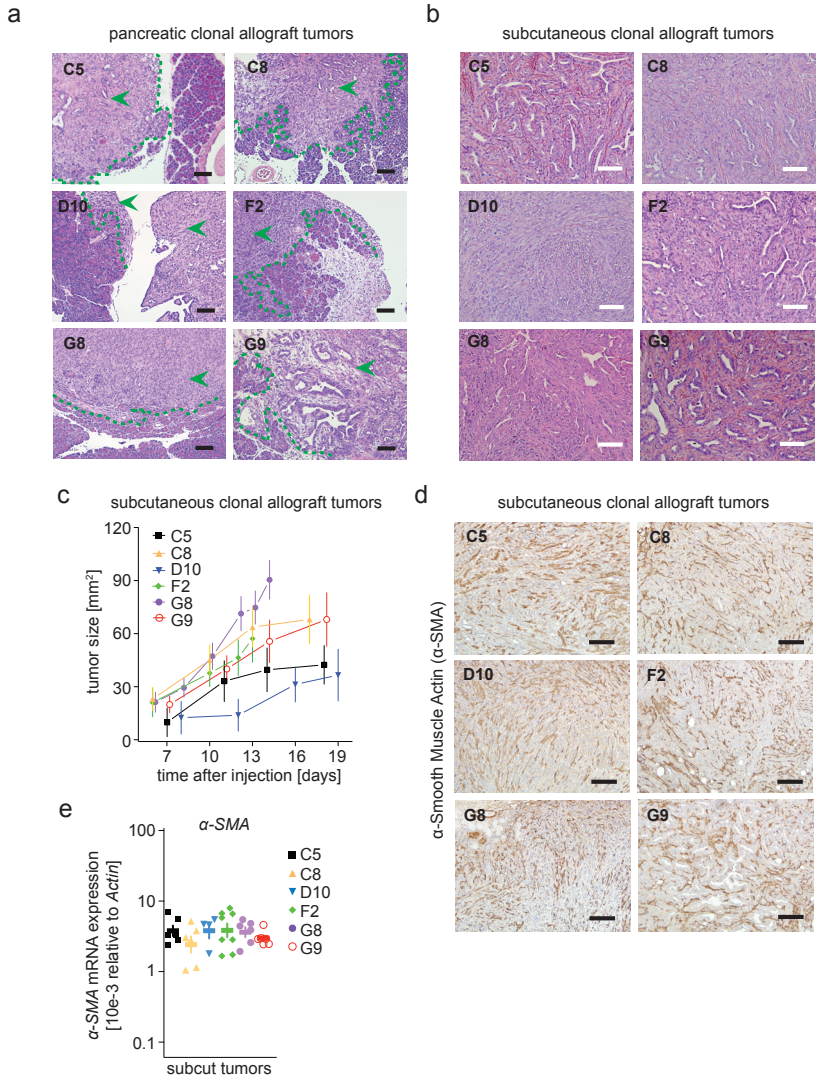

Supplementary Figure 3. Growth of clonal allograft tumors

a. Images of H&E stained FFPE pancreatic clonal allograft tumors. One million clonal cells were injected intraperitoneally into compatible immune competent mice and allowed to form tumors. Green dashed lines indicate the invasive cancer margins into healthy pancreas tissue. Green arrows indicate cancer. Scale bar =100 μm.

b. Images of H&E stained FFPE subcutaneous clonal allograft tumors. One million clonal cells were injected subcutaneously into the flanks of compatible immune competent mice. Scale bar =100 μm.

c. Growth curves of the clonal subcutaneous allograft tumors.

d. Immunohistochemical staining for α-Smooth Muscle Actin protein in FFPE subcutaneous clonal allograft tumors. Scale bar =100 μm.

e. Expression of α-Smooth Muscle Actin mRNA in subcutaneous clonal allograft tumors by qRT-PCR. The expression is normalized to beta-Actin. Note the log scale for the Y-axis. Error bars are SEM of 2 replicate measurements in ≥2 tumors per clonal cell line.

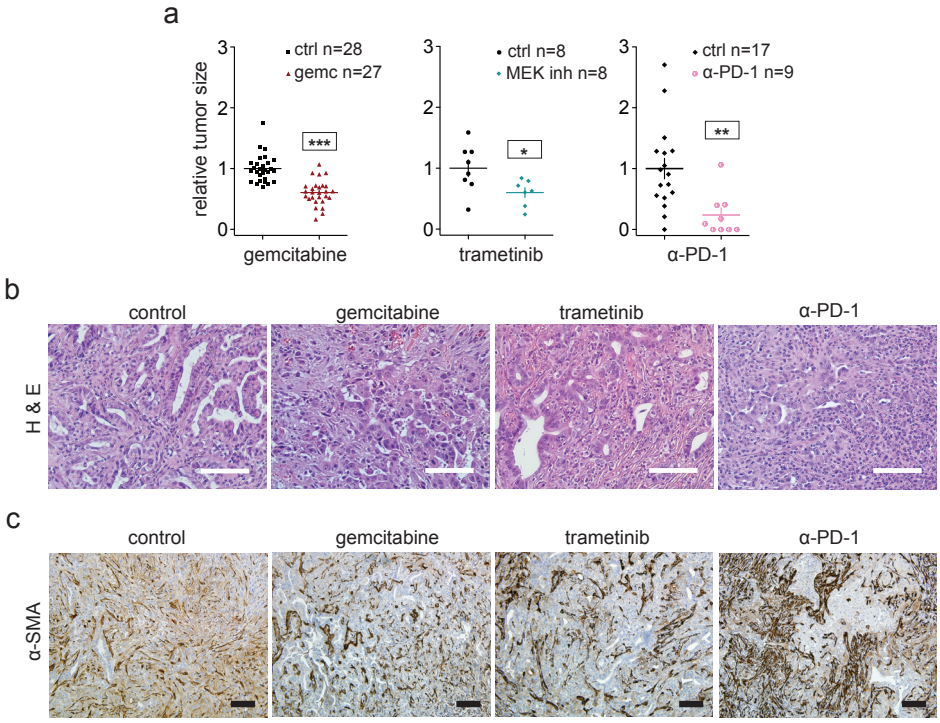

Supplementary Figure 4. Drug effects on growth of heterogeneous tumors.

a. Relative size of the subcutaneous clone mix allograft tumors. One million cells of the PDAC clone mixture were injected subcutaneously into the flanks of compatible immune competent mice. When tumors had established, mice were treated for 2 weeks with either vehicle control, 4 injections of 250 µg rat anti-mouse-PD-1 mAb, 7 injections of 40 mg/kg gemcitabine, or daily oral gavage with 0.5 mg/kg trametinib. The relative tumor size is shown per treatment group. Maximal growth inhibition was reached at day 5 for gemcitabine and trametinib. and at day 10 of α-PD-1. Error bars are SEM, ***p<0.0001; *p=0.032 **p=0.0054; versus the respective control group.

b, c. Representative , H&E (b), or α-Smooth Muscle Actin stained (c) subcutaneous allograft tumors at the end of different treatments indicated. Scale bar =100 µm.

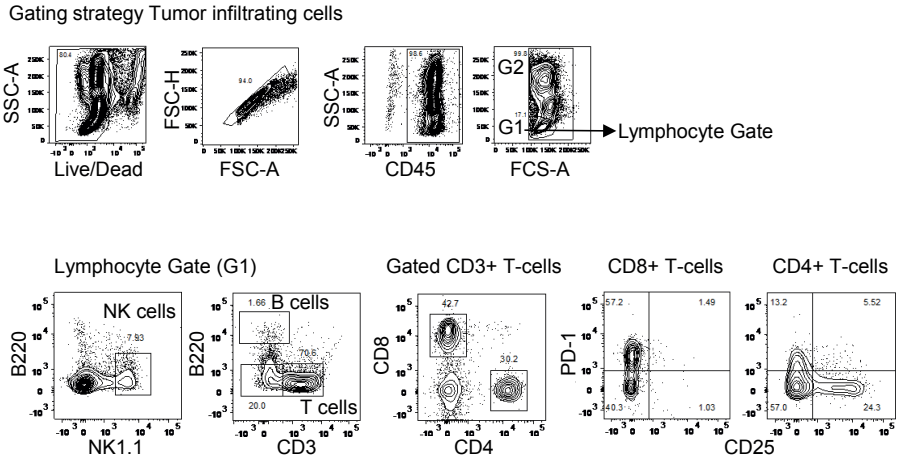

Supplementary Figure 5. Gating strategy in the flow cytometry analysis of tumor infiltrating lymphocytes. Tumor infiltrating cells were gated on time, FCS-SSC and live cells. Hematopoietic cells were selected by CD45 expression. Lymphocytes subsets were gated based on expression of: NK cells (NK1.1+), B cells (B220+), T cells (CD3+). CD4 T cells (CD3+CD4+) and CD8 T cells (CD3+CD8+) were further analyzed by surface expression of PD-1 and CD25.

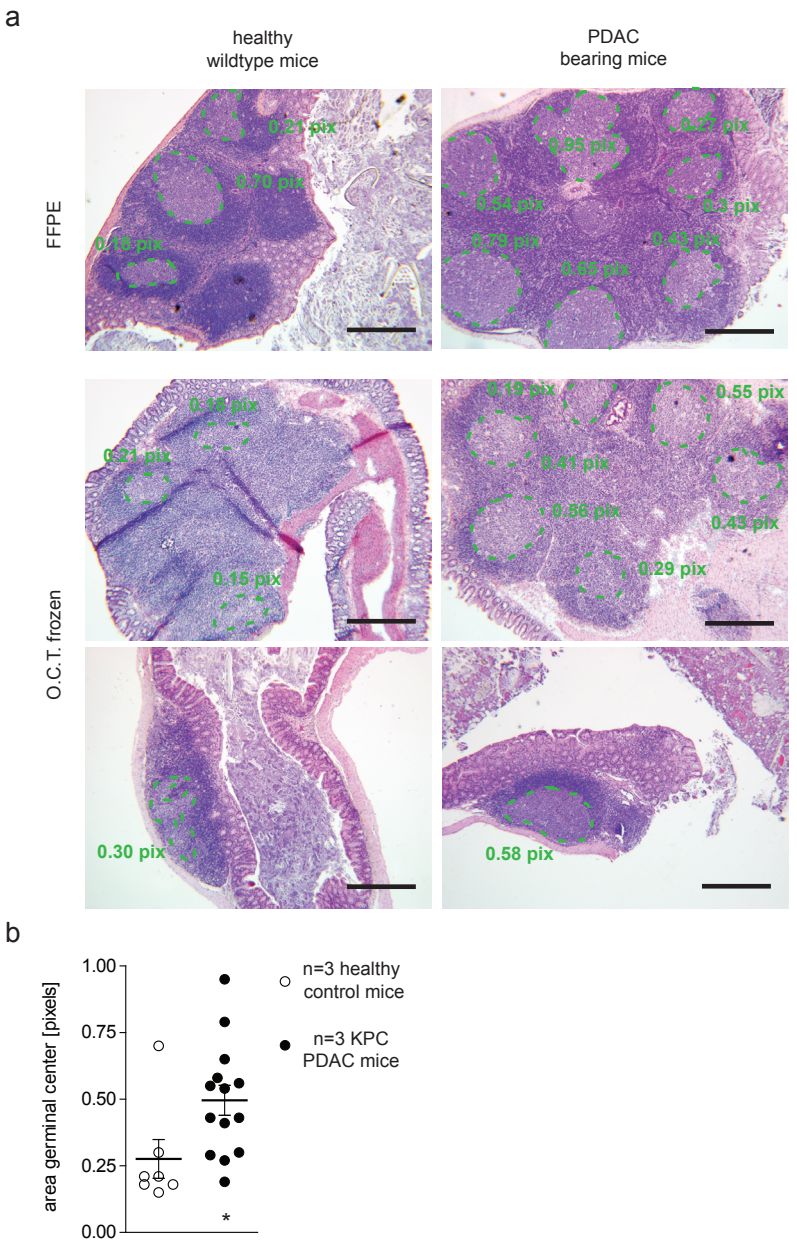

Supplementary Figure 6. Mouse ceacal patch derived T-lymphocytes

a. Images of mouse ceacal patches (equivalent to human vermiform appendix) stained with H&E. Ceacal patches from n=3 healthy immune competent mice and from n=3 KPC mice were either formalin fixed or frozen in O.C.T cryo embedding media, and sectioned. Green dashed lines encircle the germinal centers of the lymphoid tissues. Scale bar = 500 μm.

b. Areas of the germinal centers in the lymphoid tissue of the caecal patches from n=3 healthy mice and n=3 PDAC bearing KPC mice. * p=0.0316 by t-test.

b

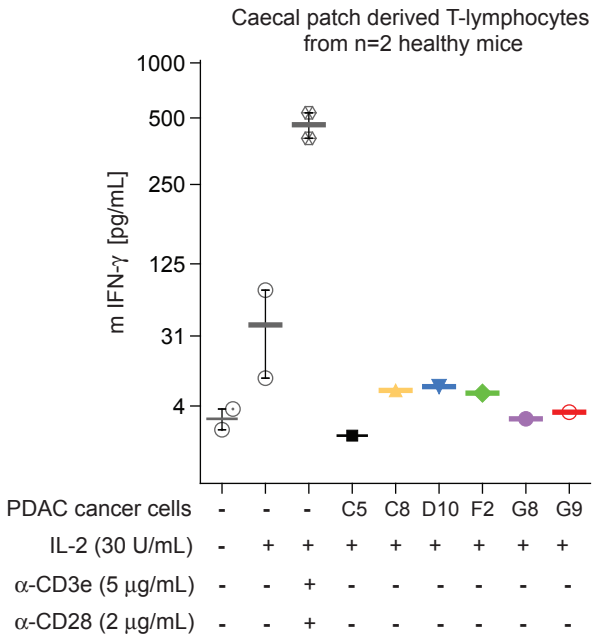

c

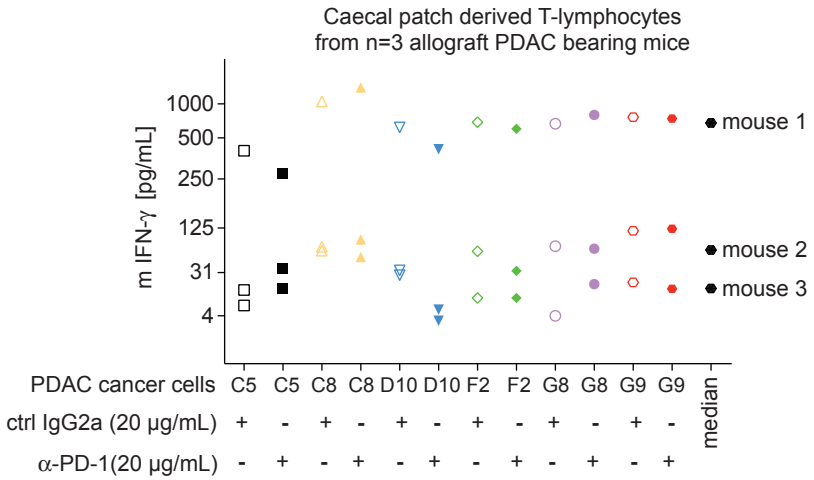

Supplementary Figure 6. Mouse ceacal patch derived T-lymphocytes

c. IFN-γ levels in the supernatant of T-lymphocytes isolated from ceacal patches of n=2 healthy mice, co-cultured with clonal PDAC cell lines, measured after 48 hours by ELISA. Note the log2 –scale for the Y-axis. Error bars are SEM of n=2 mice.

d. IFN-γ levels in the supernatant of primed appendix T-lymphocytes isolated from n=3 mice bearing mixed allograft PDAC tumors, co-cultured with the clonal PDAC cell lines in vitro, measured after 48 hours by ELISA. Note the log2 scale for the y-axis.

REFERENCES

1. Vincent, A., Herman, J., Schulick, R. et al. (2011) Pancreatic cancer. *Lancet* 378, 607-620
2. Oettle, H., Post, S., Neuhaus, P. et al. (2007) Adjuvant chemotherapy with gemcitabine vs observation in patients undergoing curative-intent resection of pancreatic cancer: a randomized controlled trial. *Jama* 297, 267-277
3. Bailey, P., Chang, D. K., Nones, K. et al. (2016) Genomic analyses identify molecular subtypes of pancreatic cancer. *Nature* 531, 47-52
4. Witkiewicz, A. K., McMillan, E. A., Balaji, U. et al. (2015) Whole-exome sequencing of pancreatic cancer defines genetic diversity and therapeutic targets. *Nat Commun* 6, 6744
5. Gilmartin, A. G., Bleam, M. R., Groy, A. et al. (2011) GSK1120212 (JTP-74057) is an inhibitor of MEK activity and activation with favorable pharmacokinetic properties for sustained in vivo pathway inhibition. *Clin Cancer Res* 17, 989-1000
6. Infante, J. R., Somer, B. G., Park, J. O. et al. (2014) A randomised, double-blind, placebo-controlled trial of trametinib, an oral MEK inhibitor, in combination with gemcitabine for patients with untreated metastatic adenocarcinoma of the pancreas. *Eur J Cancer* 50, 2072-2081
7. Greten, F. R. (2014) YAP1 takes over when oncogenic K-Ras slumbers. *Cell* 158, 11-12
8. Zhang, W., Nandakumar, N., Shi, Y. et al. (2014) Downstream of mutant KRAS, the transcription regulator YAP is essential for neoplastic progression to pancreatic ductal adenocarcinoma. *Sci Signal* 7, ra42
9. Aparicio, S. & Caldas, C. (2013) The implications of clonal genome evolution for cancer medicine. *N Engl J Med* 368, 842-851
10. Burrell, R. A., McGranahan, N., Bartek, J. et al. (2013) The causes and consequences of genetic heterogeneity in cancer evolution. *Nature* 501, 338-345
11. Kim, M. S., Zhong, Y., Yachida, S. et al. (2014) Heterogeneity of pancreatic cancer metastases in a single patient revealed by quantitative proteomics. *Mol Cell Proteomics* 13, 2803-2811
12. Bozic, I., Reiter, J. G., Allen, B. et al. (2013) Evolutionary dynamics of cancer in response to targeted combination therapy. *Elife* 2, e00747
13. Saunders, N. A., Simpson, F., Thompson, E. W. et al. (2012) Role of intratumoural heterogeneity in cancer drug resistance: molecular and clinical perspectives. *EMBO Mol Med* 4, 675-684
14. Bhang, H. E., Ruddy, D. A., Krishnamurthy Radhakrishna, V. et al. (2015) Studying clonal dynamics in response to cancer therapy using high-complexity barcoding. *Nat Med* 21, 440-448
15. Jamal-Hanjani, M., Quezada, S. A., Larkin, J. et al. (2015) Translational implications of tumor heterogeneity. *Clin Cancer Res* 21, 1258-1266
16. Kleppe, M. & Levine, R. L. (2014) Tumor heterogeneity confounds and illuminates: assessing the implications. *Nat Med* 20, 342-344
17. Beckman, R. A., Schemmann, G. S. & Yeang, C. H. (2012) Impact of genetic dynamics and single-cell heterogeneity on development of nonstandard personalized medicine strategies for cancer. *Proc Natl Acad Sci U S A* 109, 14586-14591
18. Neesse, A., Algul, H., Tuveson, D. A. et al. (2015) Stromal biology and therapy in pancreatic cancer: a changing paradigm. *Gut* 64, 1476-1484
19. Ozdemir, B. C., Pentcheva-Hoang, T., Carstens, J. L. et al. (2014) Depletion of carcinoma-associated fibroblasts and fibrosis induces immunosuppression and accelerates pancreas cancer with reduced survival. *Cancer Cell* 25, 719-734
20. Rhim, A. D., Oberstein, P. E., Thomas, D. H. et al. (2014) Stromal elements act to restrain, rather than support, pancreatic ductal adenocarcinoma. *Cancer Cell* 25, 735-747

21. Muerkoster, S., Wegehenkel, K., Arlt, A. et al. (2004) Tumor stroma interactions induce chemoresistance in pancreatic ductal carcinoma cells involving increased secretion and paracrine effects of nitric oxide and interleukin-1beta. *Cancer Res* 64, 1331-1337
22. Binenbaum, Y., Na'ara, S. & Gil, Z. (2015) Gemcitabine resistance in pancreatic ductal adenocarcinoma. *Drug Resist Updat* 23, 55-68
23. Sainz, B., Jr., Alcala, S., Garcia, E. et al. (2015) Microenvironmental hCAP-18/LL-37 promotes pancreatic ductal adenocarcinoma by activating its cancer stem cell compartment. *Gut* 64, 1921-1935
24. Nielsen, M. F., Mortensen, M. B. & Detlefsen, S. (2016) Key players in pancreatic cancer-stroma interaction: Cancer-associated fibroblasts, endothelial and inflammatory cells. *World J Gastroenterol* 22, 2678-2700
25. Feig, C., Jones, J. O., Kraman, M. et al. (2013) Targeting CXCL12 from FAP-expressing carcinoma-associated fibroblasts synergizes with anti-PD-L1 immunotherapy in pancreatic cancer. *Proc Natl Acad Sci U S A* 110, 20212-20217
26. Heppner, G. H. (1984) Tumor heterogeneity. *Cancer Res* 44, 2259-2265
27. Heppner, G. H. (1991) Cell-to-cell interaction in regulating diversity of neoplasms. *Semin Cancer Biol* 2, 97-103
28. Marusyk, A., Tabassum, D. P., Altrock, P. M. et al. (2014) Non-cell-autonomous driving of tumour growth supports sub-clonal heterogeneity. *Nature* 514, 54-58
29. Miller, B. E., Miller, F. R. & Heppner, G. H. (1981) Interactions between tumor subpopulations affecting their sensitivity to the antineoplastic agents cyclophosphamide and methotrexate. *Cancer Res* 41, 4378-4381
30. Zhao, B., Hemann, M. T. & Lauffenburger, D. A. (2014) Intratumor heterogeneity alters most effective drugs in designed combinations. *Proc Natl Acad Sci U S A* 111, 10773-10778
31. Hingorani, S. R., Wang, L., Multani, A. S. et al. (2005) Trp53R172H and KrasG12D cooperate to promote chromosomal instability and widely metastatic pancreatic ductal adenocarcinoma in mice. *Cancer Cell* 7, 469-483
32. Li, H. & Durbin, R. (2009) Fast and accurate short read alignment with Burrows-Wheeler transform. *Bioinformatics* 25, 1754-1760
33. McKenna, A., Hanna, M., Banks, E. et al. (2010) The Genome Analysis Toolkit: a MapReduce framework for analyzing next-generation DNA sequencing data. *Genome Res* 20, 1297-1303
34. Sharif, G. M., Schmidt, M. O., Yi, C. et al. (2015) Cell growth density modulates cancer cell vascular invasion via Hippo pathway activity and CXCR2 signaling. *Oncogene* 34, 5879-5889
35. Maddipati, R. & Stanger, B. Z. (2015) Pancreatic Cancer Metastases Harbor Evidence of Polyclonality. *Cancer Discov* 5, 1086-1097
36. Yip-Schneider, M. T., Lin, A., Barnard, D. et al. (1999) Lack of elevated MAP kinase (Erk) activity in pancreatic carcinomas despite oncogenic K-ras expression. *Int J Oncol* 15, 271-279
37. Yeh, J. J., Routh, E. D., Rubinas, T. et al. (2009) KRAS/BRAF mutation status and ERK1/2 activation as biomarkers for MEK1/2 inhibitor therapy in colorectal cancer. *Mol Cancer Ther* 8, 834-843
38. Sakakura, C., Hagiwara, A., Shirahama, T. et al. (1999) Infrequent activation of mitogen-activated protein kinase in human colon cancers. *Hepatogastroenterology* 46, 2831-2834
39. Drifka, C. R., Loeffler, A. G., Mathewson, K. et al. (2016) Highly aligned stromal collagen is a negative prognostic factor following pancreatic ductal adenocarcinoma resection. *Oncotarget* 7, 76197-76213
40. Egeblad, M., Rasch, M. G. & Weaver, V. M. (2010) Dynamic interplay between the collagen scaffold and tumor evolution. *Curr Opin Cell Biol* 22, 697-706
41. Whatcott, C. J., Diep, C. H., Jiang, P. et al. (2015) Desmoplasia in Primary Tumors and Metastatic Lesions of Pancreatic Cancer. *Clin Cancer Res* 21, 3561-3568

42. Campbell, P. J., Yachida, S., Mudie, L. J. et al. (2010) The patterns and dynamics of genomic instability in metastatic pancreatic cancer. *Nature* 467, 1109-1113
43. Yachida, S., Jones, S., Bozic, I. et al. (2010) Distant metastasis occurs late during the genetic evolution of pancreatic cancer. *Nature* 467, 1114-1117
44. Collisson, E. A., Trejo, C. L., Silva, J. M. et al. (2012) A central role for RAF-->MEK-->ERK signaling in the genesis of pancreatic ductal adenocarcinoma. *Cancer Discov* 2, 685-693
45. Galluzzi, L., Senovilla, L., Zitvogel, L. et al. (2012) The secret ally: immunostimulation by anticancer drugs. *Nat Rev Drug Discov* 11, 215-233
46. Kidd, B. A., Wroblewska, A., Boland, M. R. et al. (2016) Mapping the effects of drugs on the immune system. *Nat Biotechnol* 34, 47-54
47. Ott, P. A. & Adams, S. (2011) Small-molecule protein kinase inhibitors and their effects on the immune system: implications for cancer treatment. *Immunotherapy* 3, 213-227
48. Sideras, K., Braat, H., Kwekkeboom, J. et al. (2014) Role of the immune system in pancreatic cancer progression and immune modulating treatment strategies. *Cancer Treat Rev* 40, 513-522
49. Clark, C. E., Hingorani, S. R., Mick, R. et al. (2007) Dynamics of the immune reaction to pancreatic cancer from inception to invasion. *Cancer Res* 67, 9518-9527
50. Chikuma, S., Terawaki, S., Hayashi, T. et al. (2009) PD-1-mediated suppression of IL-2 production induces CD8+ T cell anergy in vivo. *J Immunol* 182, 6682-6689
51. Shevach, E. M. (2001) Certified professionals: CD4(+)CD25(+) suppressor T cells. *J Exp Med* 193, F41-46
52. Alkadhi, S., Kunde, D., Cheluvappa, R. et al. (2014) The murine appendiceal microbiome is altered in spontaneous colitis and its pathological progression. *Gut Pathog* 6, 25
53. Watson Ng, W. S., Hampartzoumian, T., Lloyd, A. R. et al. (2007) A murine model of appendicitis and the impact of inflammation on appendiceal lymphocyte constituents. *Clin Exp Immunol* 150, 169-178
54. Halle, S., Halle, O. & Forster, R. (2017) Mechanisms and Dynamics of T Cell-Mediated Cytotoxicity In Vivo. *Trends Immunol* 6,432-443
55. Topalian, S. L., Taube, J. M., Anders, R. A. et al. (2016) Mechanism-driven biomarkers to guide immune checkpoint blockade in cancer therapy. *Nat Rev Cancer* 16, 275-287
56. Miller, B. E., Miller, F. R., Leith, J. et al. (1980) Growth interaction in vivo between tumor subpopulations derived from a single mouse mammary tumor. *Cancer Res* 40, 3977-3981
57. Roesch, A., Fukunaga-Kalabis, M., Schmidt, E. C. et al. (2010) A temporarily distinct subpopulation of slow-cycling melanoma cells is required for continuous tumor growth. *Cell* 141, 583-594
58. Cassidy, J. W., Caldas, C. & Bruna, A. (2015) Maintaining Tumor Heterogeneity in Patient-Derived Tumor Xenografts. *Cancer Res* 75, 2963-2968
59. Nakasone, E. S., Askautrud, H. A., Kees, T. et al. (2012) Imaging tumor-stroma interactions during chemotherapy reveals contributions of the microenvironment to resistance. *Cancer Cell* 21, 488-503
60. Straussman, R., Morikawa, T., Shee, K. et al. (2012) Tumour micro-environment elicits innate resistance to RAF inhibitors through HGF secretion. *Nature* 487, 500-504
61. Majumder, B., Baraneedharan, U., Thiyagarajan, S. et al. (2015) Predicting clinical response to anticancer drugs using an ex vivo platform that captures tumour heterogeneity. *Nat Commun* 6, 6169
62. McMillin, D. W., Delmore, J., Weisberg, E. et al. (2010) Tumor cell-specific bioluminescence platform to identify stroma-induced changes to anticancer drug activity. *Nat Med* 16, 483-489
63. Bartlett, R., Everett, W., Lim, S. et al. (2014) Personalized in vitro cancer modeling - fantasy or reality? *Transl Oncol* 7, 657-664
64. Miller, F. R. & Heppner, G. H. (1979) Immunologic heterogeneity of tumor cell subpopulations from a single mouse mammary tumor. *J Natl Cancer Inst* 63, 1457-1463

65. Topalian, S. L., Hodi, F. S., Brahmer, J. R. et al. (2012) Safety, activity, and immune correlates of anti-PD-1 antibody in cancer. *N Engl J Med* 366, 2443-2454
66. Borghaei, H., Paz-Ares, L., Horn, L. et al. (2015) Nivolumab versus Docetaxel in Advanced Nonsquamous Non-Small-Cell Lung Cancer. *N Engl J Med* 373, 1627-1639
67. Kreso, A., O'Brien, C. A., van Galen, P. et al. (2013) Variable clonal repopulation dynamics influence chemotherapy response in colorectal cancer. *Science* 339, 543-548
68. Jiang, Y., Li, Y. & Zhu, B. (2015) T-cell exhaustion in the tumor microenvironment. *Cell Death Dis* 6, e1792